Astron. Nachr./AN **32X** 2004 X, XXX-XXX

arXiv:astro-ph/0505306v1 14 May 2005

Homeoidally striated density profiles: sequences of virial equilibrium configurations with constant anisotropy parameters

R. CAIMMI AND C. MARMO

Dipartimento di Astronomia, Università di Padova,
Vicolo Osservatorio 2, I-35122 Padova, Italy
e-mail: caimmi@pd.astro.it

Received..... Accepted.....

Abstract. The formulation of the tensor virial equations is generalized to unrelaxed configurations, where virial equilibrium does not coincide with dynamical (or hydrostatic) equilibrium. Special classes of homeoidally striated ellipsoids are shown to exhibit similar properties as Jacobi ellipsoids, and reduce to Jacobi ellipsoids in the limiting situation of homogeneous matter distribution, rigid rotation, and isotropic residual (i.e. other than systematic rotation) velocity distribution. Accordingly, the above mentioned density profiles are defined as homeoidally striated, Jacobi ellipsoids. Further investigation is devoted to the generation of sequences of virial equilibrium configurations. Sequences with constant anisotropy parameters are studied with more detail, including both flattened and elongated, triaxial (in particular, both oblate and prolate, axisymmetric) configurations, and the determination of the related bifurcation points. The explicit expression of a number of rotation parameters, used in literature, and the ratio of rms rotational to rms residual velocity, is also calculated. An application is made to dark matter haloes hosting giant galaxies ($M \approx 10^{12}\mathrm{m}_{\odot}$), with regard to assigned initial and final configuration, following and generalizing to many respects a procedure conceived by Thuan & Gott (1975). The dependence of the limiting axis ratios, below which no configuration is allowed for the sequence under consideration, on the change in mass, total energy, and angular momentum, during the evolution, is illustrated in some representative situations. The dependence of the axis ratios, ϵ_{31} and ϵ_{21}, on a parameter, related to the initial conditions of the density perturbation, is analysed in connection with a few special cases. The same is done for the rotation

parameters and the ratio of rms rotational to rms residual velocity. Within the range of the rotation parameter, $\exp_{10}(\log\lambda \mp \sigma_{\log\lambda}) = \exp_{10}(-1.3761 \mp 0.500)$, consistent with high-resolution numerical simulations, the shape of dark matter haloes is mainly decided by the amount of anisotropy in residual velocity distribution (the above formula uses the general notation, $\exp_a(x) = a^x$, where the special case, $a = \mathrm{e}$, reduces to the standard notation). On the other hand, the contribution of rotation has only a minor effect on the meridional plane, and no effect on the equatorial plane, as bifurcation points occur for larger values of λ. To this respect, dark matter haloes are found to resemble giant elliptical galaxies.

Key words: Cosmology: dark matter - galaxies: evolution - galaxies: formation - galaxies:haloes - galaxies: structure.

1. Introduction

Homeoidally striated density profiles make a useful tool in the description of self-gravitating fluids on many respects. First, the related potential-energy tensors are expressed as the product between a profile factor and a shape factor. Accordingly, a physical parameter which depends on the ratio between different components of a same potential-energy tensor, is a function of the axis ratios only (Roberts 1962). In addition, the constraints for homeoidally striated ellipsoids, in connection with both equilibrium and stability, are left unchanged with respect to the special case of homogeneous configurations with same shape (e.g., Binney 1978; Pacheco et al. 1989). Second, a criterion for an upper limit to the point of bifurcation from axisymmetric to triaxial configurations, is formally identical for collisional and collisionless fluids (Wiegandt 1982a). On the other hand, a condition for dynamical stability depends on the degree of anisotropy of peculiar velocity distribution (Wiegandt 1982b). In this framework, additional features may be included, such as vorticity and streaming motions (e.g., Pacheco et al. 1986, 1989; Busarello et al. 1989, 1990; and further references therein).

For the purpose of the current attempt, our attention shall be restricted to the simplest case where both vorticity and streaming motions are not explicitly investigated, and only the contribution from systematic rotation is considered separately. Owing to a generalization of Dedekind's theorem, to each configuration with no vorticity and assigned angular velocity, Ω, will correspond an "adjoint" configuration with same boundary and distribution of peculiar velocity, but with no rotation and vorticity parameter, $Z = \Omega$ (Pacheco et al. 1989). Accordingly, to each transition from an initial to a final, (at least rigidly) rotating configuration, will correspond a transition from an initial to a final, vorticating, adjoint configuration.

The choice of homeoidally striated density profiles as a valid approximation to the description of self-gravitating fluids, is motivated by two main reasons. *In primis*, most astronomical

©WILEY-VCH Verlag Berlin GmbH, 13086 Berlin, Germany 2004 0044-6337/04/32201-0223 $ 17.50+.50/0

bodies exhibit ellipsoidal-like shapes and isopycnic surfaces. *Secundo*, homeoidally striated ellipsoids approximate to a first extent collisional and collisionless, self-gravitating fluids (e.g., Vandervoort 1980; Vandervoort & Welty 1981; Lai et al. 1993), at least with regard to global properties, involving averages on the whole mass distribution. On the other hand, some caution must be used in dealing with local properties, involving values *in situ*. For instance, velocity dispersion values measured in the central region of a galaxy, can be significantly different for structurally identical systems (and so characterized by identical, global velocity dispersions), due to different orbital structures.

Though classical investigations have been restricted to figures of dynamical (or hydrostatic) equilibrium such as MacLaurin spheroids and Jacobi ellipsoids (e.g., Jeans 1929, Chaps. VIII-IX; Chandrasekhar 1966, Chaps. 5-8), still the current attempt may be generalized to figures of virial equilibrium. Let us define virial equilibrium as characterized by the validity of the virial theorem, and relaxed and unrelaxed configurations as systems where virial equilibrium does and does not coincide, respectively, with dynamical (or hydrostatic) equilibrium.

In the special case of relaxed configurations, the virial theorem is usually formulated by setting the sum of the potential energy, and twice the kinetic energy, equal to zero. On the other hand, the above mentioned relation no longer holds for unrelaxed configurations, and a more general formulation of the virial equations is needed. To this aim, our attention shall be limited to homeoidally striated density profiles, where the rotational velocity field is subjected to a number of necessary restrictions. Then the related sequences of virial equilibrium configurations with constant rotation and anisotropy parameters, can be studied in detail.

An extension of the formulation of the virial equations to unrelaxed configurations, and the investigation of sequences where both rotation and anisotropy parameters remain unchanged, make the aim of the current paper. As an application of the theory, a procedure to establish mutual connection between physical parameters related to assigned initial and final state of a density perturbation, may be generalized to many respects.

About a quarter of century ago, Thuan & Gott (1975) idealized elliptical galaxies as MacLaurin spheroids, resulting from virialization after cosmological expansion and subsequent collapse and relaxation of their parent density perturbations. Unexpectively, the above mentioned model provided an answer to the question, why there are no elliptical galaxies more flattened than E7. The method is based on the knowledge of an initial configuration, assumed to be at turnaround, and a final configuration, assumed to be a MacLaurin spheroid. A generalization to a somewhat more arbitrary initial and final configuration, and to other respects, is expected to be useful for e.g., comparison with (i) results of numerical simulations, and (ii) observations.

More specifically, the problem may be formulated as follows. Let the physical parameters of a density perturbation be specified at a selected, initial and final configuration, at redshift z_i and z_f, respectively, provided $z_{rec} \geq z_i \geq z_f \geq z_{vir}$, where the indices, rec and vir,

denote recombination and virialization, respectively. Let the density profile be assigned, and the isopycnic surfaces, i.e. the surfaces of equal density, be similar and similarly placed ellipsoids. Let the rotational velocity field, and the amount of anisotropy in residual (in particular, peculiar) velocity distribution, also be specified. Under the above mentioned assumptions, determine the shape of the final configuration, and the related physical parameters.

The generalization of Thuan & Gott (1975) procedure to a special class of homeoidally striated ellipsoids, together with an application to dark matter haloes hosting giant galaxies ($M \approx 10^{12}\mathrm{m}_{\odot}$), makes a specific application of the theory outlined above. It shall be analysed in the present attempt.

The current paper is organized as follows. The general theory of homeoidally striated density profiles, and the results of interest to the aim of this investigation, are outlined in Sect. 2. The properties of a special class of configurations, defined as homeoidally striated Jacobi ellipsoids, are studied in Sect. 3 where, in particular, the explicit expressions of some rotation parameters, known in literature, are derived. Then sequences of virial equilibrium configurations are determined, where both rotation and anisotropy parameters remain unchanged. A generalization of the procedure followed by Thuan & Gott (1975) to homeoidally striated density profiles is performed in Sect. 4, and a number of special situations are also investigated. Furthermore, an application is made to dark matter haloes hosting giant galaxies, and the results are presented and discussed. Some concluding remarks are drawn in Sect. 5, and a few arguments are treated with more detail in the Appendix.

2. General theory

A general theory for homeoidally striated density profiles has been developed in earlier approaches (Roberts 1962; Caimmi 1993a; Caimmi & Marmo 2003, hereafter quoted as CM03), and an interested reader is addressed therein for deeper insight. What is relevant for the current investigation, shall be mentioned and further developed here.

The isopycnic surfaces are defined by the following law:

$$\rho = \rho_0 f(\xi) \ ; \quad f(1) = 1 \ ; \quad \rho_0 = \rho(1) \ ; \tag{1a}$$

$$\xi = \frac{r}{r_0} \ ; \quad 0 \leq \xi \leq \Xi \ ; \quad \Xi = \frac{R}{r_0} \ ; \tag{1b}$$

where ρ_0, r_0 are a scaling radius and a scaling density, respectively, related to a reference isopycnic surface, and Ξ, R, correspond to the boundary. By "radius" we intend here the radial coordinate of a generic point on a generic isopycnic surface. The radius changes - in general - passing from one point to one other, along a fixed isopycnic surface, and it may coincide - in particular - with a semiaxis of the related ellipsoid.

Let Σ_1 and Σ_2 be generic isopycnic surfaces belonging to a homeoidally striated density profile, and r_1, r_2, generic radii along the same direction. It can be shown (e.g., CM03) that the ratio, r_1/r_2, is independent of direction. The above result holds, in particular, in the special

case where an isopycnic surface coincides with the reference isopycnic surface, according to Eq. (1b). In other words the scaled radius, ξ, is defined as the ratio between the radius of the isopycnic surface under consideration, along a generic direction, and the radius of the reference isopycnic surface, along the same direction.

The mass, the inertia tensor, and the self-energy tensor, are:

$$M = \nu_{mas} M_0 \ ; \tag{2}$$

$$I_{pq} = \delta_{pq} \nu_{inr} M a_p^2 \ ; \tag{3}$$

$$(E_{sel})_{pq} = -\frac{GM^2}{a_1} \nu_{sel} (B_{sel})_{pq} \ ; \tag{4}$$

$$(B_{sel})_{pq} = \delta_{pq} \epsilon_{p2} \epsilon_{p3} A_p \ ; \quad B_{sel} = \sum_{s=1}^{3} \epsilon_{s2} \epsilon_{s3} A_s \ ; \tag{5}$$

where δ_{pq} is the Kronecker symbol; G is the constant of gravitation; ν_{mas}, ν_{inr}, ν_{sel}, are profile factors i.e. depend only on the density profile via the scaled radius, Ξ; a_1, a_2, a_3, are semiaxes; $\epsilon_{pq} = a_p/a_q$ are axis ratios; A_1, A_2, A_3, are shape factors i.e. depend only on the axis ratios; and M_0 is the mass of a homogeneous ellipsoid with same density and boundary as the reference isopycnic surface:

$$M_0 = \frac{4\pi}{3} \rho_0 a_{01} a_{02} a_{03} \ ; \tag{6}$$

where a_{01}, a_{02}, a_{03}, are the semiaxes of the ellipsoid bounded by the reference isopycnic surface. Owing to a different normalization of the physical quantities, the profile parameters, ν, have a different expression with respect to CM03. For further details, see Appendix A. Values of shape factors related to limiting configurations (round, oblate, prolate, flat, and oblong) are derived in Appendix B.

In dealing with angular momentum and rotational energy, the preservation of (triaxial) ellipsoidal shape imposes severe constraints on the rotational velocity field. Leaving an exhaustive investigation to more refined approaches, our attention shall be limited here to a restricted number of special cases, namely: (i) rigid rotation about a principal axis, and (ii) differential rotation about a symmetry axis. By "rotation" it is intended, of course, circular rotation.

In the special case of rigid rotation about a principal axis, let it be x_3, the angular-momentum vector and the rotational-energy tensor are:

$$J_s = \delta_{s3} (I_{pp} + I_{qq}) \Omega_s = \delta_{s3} \nu_{inr} M a_p (1 + \epsilon_{qp}^2) (v_{rot})_p \ ; \quad p \neq q \neq s \ ; \tag{7}$$

$$\begin{aligned} (E_{rot})_{pq} &= \frac{1}{2} I_{pq} \delta_{s3} \Omega_s^2 = \frac{1}{2} \delta_{s3} \delta_{pq} (1 - \delta_{ps}) \nu_{inr} M a_p^2 \Omega^2 \\ &= \frac{1}{2} \delta_{s3} \delta_{pq} (1 - \delta_{ps}) \nu_{inr} M \left[(v_{rot})_p \right]^2 \ ; \qquad p \neq s \ ; \qquad q \neq s \ ; \end{aligned} \tag{8}$$

where Ω is the angular velocity related to the axis, x_3, and $(v_{rot})_p$ is the rotational velocity at the end of the semiaxis, a_p, $p = 1, 2$.

The module of the above vector and the trace of the above tensor, which make the related angular momentum and rotational energy, respectively, read:

$$J = \nu_{inr} M a_p^2 (1 + \epsilon_{qp}^2) \Omega = \nu_{inr} M a_p (1 + \epsilon_{qp}^2) (v_{rot})_p \ ; \tag{9}$$

$$E_{rot} = \frac{1}{2} \nu_{inr} M a_p^2 (1 + \epsilon_{qp}^2) \Omega^2 = \frac{1}{2} \nu_{inr} M (1 + \epsilon_{qp}^2) \left[(v_{rot})_p \right]^2 \ ; \tag{10}$$

for further details, see CM03.

In the special case of differential rotation about a symmetry axis, let it be x_3, our attention shall be restricted to rotational (with respect to x_3 axis) velocity distributions which obey the law:

$$\frac{v_{rot}(r,\theta)}{v_{rot}(R,\theta)} = \frac{v_{rot}(a'_p,0)}{v_{rot}(a_p,0)} \ ; \tag{11}$$

or equivalently, to angular (with respect to x_3 axis) velocity distributions which obey the law:

$$\frac{\Omega(r,\theta)}{\Omega(R,\theta)} = \frac{\Omega(a'_p,0)}{\Omega(a_p,0)} \ ; \tag{12}$$

where (r,θ), (R,θ), represent a point on a generic isopycnic surface and on the boundary, respectively, along a fixed radial direction, and $(a'_p,0)$, $(a_p,0)$, $p=1,2$, represent the end of the corresponding equatorial semiaxis. It is worth noticing that, in particular, either rotational or angular velocity are allowed to be constant everywhere.

The equivalence of Eqs. (11) and (12) is owing to the similarity between isopycnic surfaces, which translates into the equivalent relations:

$$\frac{r}{R} = \frac{a'}{a} \ ; \quad \frac{r}{r_0} = \frac{a'}{a_0} \ ; \tag{13}$$

as outlined above in connection with ellipsoidal configurations.

The angular-momentum vector and the rotational-energy tensor are:

$$J_s = 2\delta_{s3}\eta_{anm}\nu_{anm}Mav_{rot} \ ; \tag{14}$$

$$(E_{rot})_{pq} = \delta_{pq}(1-\delta_{p3})\eta_{rot}\nu_{rot}Mv_{rot}^2 \ ; \tag{15}$$

where v_{rot} is the rotational velocity at the end of the equatorial semiaxis, a; η_{anm}, η_{rot}, depend on the boundary and on the distribution of angular velocity therein, and then may be conceived as shape factors; on the other hand, ν_{anm}, ν_{rot}, depend on the density profile and on the radial distribution of angular velocity, and then are genuine profile factors.

The module of the above vector and the trace of the above tensor, which make the related angular momentum and rotational energy, respectively, read:

$$J = 2\eta_{anm}\nu_{anm}Mav_{rot} \ ; \tag{16}$$

$$E_{rot} = 2\eta_{rot}\nu_{rot}Mv_{rot}^2 \ ; \tag{17}$$

for further details, see CM03.

To save space, let us merge Eqs. (7) and (14); (8) and (15); as:

$$J_s = \delta_{s3}\eta_{anm}\nu_{anm}Ma_p(1+\epsilon_{qp}^2)(v_{rot})_p \ ; \quad p\neq q\neq s \ ; \tag{18}$$

$$(E_{rot})_{pq} = \delta_{pq}(1-\delta_{p3})\eta_{rot}\nu_{rot}M\left[(v_{rot})_p\right]^2 \ ; \tag{19}$$

and Eqs. (9) and (16); (10) and (17); as:

$$J = \eta_{anm}\nu_{anm}M(1+\epsilon_{21}^2)a_1(v_{rot})_1 \ ; \tag{20}$$

$$E_{rot} = \eta_{rot}\nu_{rot}M(1+\epsilon_{21}^2)\left[(v_{rot})_1\right]^2 \ ; \tag{21}$$

respectively, where $\eta_{anm}\nu_{anm} = \nu_{inr}$ and $\eta_{rot}\nu_{rot} = \nu_{inr}/2$ in the special case of rigid rotation; for further details, see CM03.

An expression of the rotational energy, E_{rot}, as a function of the angular momentum, J, is obtained by the combination of Eqs. (20) and (21), as:

$$E_{rot} = \frac{J^2}{Ma_1^2}\nu_{ram}B_{ram} \ ; \tag{22a}$$

$$\nu_{ram} = \frac{\nu_{rot}}{\nu_{anm}^2} \ ; \tag{22b}$$

$$(B_{ram})_{pq} = \delta_{pq}(1-\delta_{p3})\frac{\eta_{rot}}{\eta_{anm}^2}\frac{\epsilon_{p1}^2}{(1+\epsilon_{21}^2)^2} \ ; \tag{22c}$$

$$B_{ram} = \frac{\eta_{rot}}{\eta_{anm}^2}\frac{1}{1+\epsilon_{21}^2} \ ; \tag{22d}$$

and the ratio of rotational to self-potential energy, taken with the positive sign, $\mathcal{E}_{rot}$, is obtained by the combination of Eqs. (4), extended to the trace of the related tensor, and (22), as:

$$\mathcal{E}_{rot} = -\frac{E_{rot}}{E_{sel}} = \frac{\nu_{ram}}{\nu_{sel}}\frac{B_{ram}}{B_{sel}}h \ ; \tag{23a}$$

$$h = \frac{J^2}{GM^3a_1} \ ; \tag{23b}$$

where both $\mathcal{E}_{rot}$ (e.g., Ostriker & Peebles 1973) and h (e.g., Caimmi 1980) may be conceived as rotation parameters.

At this stage, we have all the ingredients for generalizing the usual formulation of the tensor virial equations (e.g., Chandrasekhar 1961, Chap. 13, §117; Brosche 1970; Brosche et al. 1983), to include unrelaxed configurations, in particular homeoidally striated density profiles.

3. The tensor virial equations for homeoidally striated density profiles

3.1. Basic theory

As outlined in Sect. 1, homeoidally striated density profiles make a useful tool in the description of self-gravitating fluids on many respects. Though classical investigations have been restricted to figures of dynamical (or hydrostatic) equilibrium such as MacLaurin spheroids and Jacobi ellipsoids (e.g., Jeans 1929, Chaps. VIII-IX; Chandrasekhar 1966, Chaps. 5-8), still the current attempt may be generalized to figures of virial equilibrium. To this respect, it is worth remembering that the virial theorem holds for values of parameters averaged over a sufficiently long time, $t \gg T$, where T is a characteristic period of the system (e.g., Landau & Lifchitz 1966, Chap. II, § 10).

Let us define virial equilibrium as characterized by the validity of the virial theorem, and relaxed and unrelaxed configurations as systems where virial equilibrium does and does not coincide, respectively, with dynamical (or hydrostatic) equilibrium. For instance, a compressible homogeneous sphere undergoing coherent oscillations, is in virial equilibrium: then the generic configuration is unrelaxed, even if a special one exists, equal in shape to its relaxed counterpart.

In the special case of relaxed configurations, the virial theorem is usually formulated by setting the sum of the potential energy, and twice the kinetic energy, equal to zero. On the

other hand, the above mentioned relation no longer holds for unrelaxed configurations, and a more general formulation of the virial equations is needed. To this aim, our attention shall be limited to homeoidally striated density profiles, where the rotational velocity field is subjected to the restrictions mentioned in Sect. 2.

With regard to unrelaxed configurations, let us define the residual kinetic-energy tensor, $(E_{res})_{pq}$, as owing to any motion other than systematic rotation e.g., random motions, streaming motions, radial motions; and the effective, residual kinetic-energy tensor, $(\tilde{E}_{res})_{pq}$, as the right amount needed for the configuration of interest to be relaxed i.e. the validity of the tensor virial equations:

$$(E_{sel})_{pq} + 2(E_{rot})_{pq} + 2(\tilde{E}_{res})_{pq} = 0 \ ; \tag{24}$$

then the components of the effective anisotropy tensor, defined as:

$$\tilde{\zeta}_{pq} = \frac{(\tilde{E}_{res})_{pq}}{\tilde{E}_{res}} \ ; \qquad p = 1,2,3 \ ; \qquad q = 1,2,3 \ ; \tag{25a}$$

$$\sum_{p=1}^{3} \tilde{\zeta}_{pp} = 1 \ ; \qquad 0 \leq \tilde{\zeta}_{pp} \leq 1 \ ; \qquad \tilde{\zeta}_{pq} = 0 \ ; \qquad p \neq q \ ; \tag{25b}$$

may be conceived as effective anisotropy parameters (with respect to the effective residual kinetic-energy tensor). Similarly, the components of the generalized anisotropy tensor, defined as:

$$\zeta_{pq} = \frac{(\tilde{E}_{res})_{pq}}{E_{res}} \ ; \qquad p = 1,2,3 \ ; \qquad q = 1,2,3 \ ; \tag{26a}$$

$$\sum_{p=1}^{3} \zeta_{pp} = \frac{\tilde{E}_{res}}{E_{res}} = \zeta \ ; \qquad 0 \leq \zeta_{pp} \leq \zeta \ ; \qquad \zeta_{pq} = 0 \ ; \qquad p \neq q \ ; \tag{26b}$$

may be conceived as generalized anisotropy parameters (with respect to the generalized residual kinetic-energy tensor).

The scalar, ζ, may be thought of as a virial index, where $\zeta = 1$ corresponds to null virial, $(E_{sel})_{pq} + 2(E_{rot})_{pq} + 2(E_{res})_{pq} = 0$ (which doe not necessarily imply a relaxed configuration), $\zeta > 1$ to negative virial, and $\zeta < 1$ to positive virial.

The combination of Eqs. (25) and (26) yields:

$$\tilde{\zeta}_{pp} = \frac{\zeta_{pp}}{\zeta} \ ; \qquad p = 1,2,3 \ ; \tag{27}$$

and the specification of the effective and generalized anisotropy parameters, $\tilde{\zeta}_{pp}$ and ζ_{pp}, and the residual kinetic energy, E_{res}, implies the specification of the effective, residual kinetic-energy tensor, $(\tilde{E}_{res})_{pq}$.

In the special case of relaxed configurations, the effective, residual and actual kinetic-energy tensors coincide, $(\tilde{E}_{res})_{pq} = (E_{res})_{pq}$, i.e. $\zeta = 1$. Then the limiting situation of relaxed configurations may directly be obtained from the results of the current Section, in the limit $\zeta \to 1$.

Using Eqs. (4), (5), (19), (22), and (26), Eq. (24) takes the more explicit expression:

$$-\nu_{sel}\frac{GM^2}{a_1}(B_{sel})_{pp} + 2\nu_{ram}\frac{J^2}{Ma_1^2}(B_{ram})_{pp} + 2\zeta_{pp}E_{res} = 0 \ ; \tag{28}$$

leaving aside the trivial case of non-diagonal terms, where they reduce to identities, $0 = 0$. The special choice, $p = 3$, reads:

$$-\nu_{sel}\frac{GM^2}{a_1}(B_{sel})_{33} + 2\zeta_{33}E_{res} = 0 \ ; \tag{29}$$

which allows the following expression of the residual kinetic energy:

$$E_{res} = \frac{1}{2}\frac{\nu_{sel}}{\zeta_{33}}\frac{GM^2}{a_1}(B_{sel})_{33} \ ; \tag{30}$$

as first outlined in dealing with MacLaurin spheroids (Brosche 1970).

The combination of Eqs. (28) and (30) yields:

$$\nu_{sel}\frac{GM^2}{a_1}\left[(B_{sel})_{qq} - \frac{\zeta_{qq}}{\zeta_{33}}(B_{sel})_{33}\right] - 2\nu_{ram}\frac{J^2}{Ma_1^2}(B_{ram})_{qq} = 0 \ ; \quad q = 1, 2 \ ; \tag{31}$$

leaving aside the trivial case, $p = 3$, where it reduces to an identity, $0 = 0$. A necessary condition for satisfiyng Eq. (31), or (24), using Eqs. (5), may be written as:

$$\frac{\zeta_{qq}}{\zeta_{33}} \leq \frac{(B_{sel})_{qq}}{(B_{sel})_{33}} = \frac{A_q}{\epsilon_{3q}^2 A_3} \ ; \qquad q = 1, 2 \ ; \tag{32}$$

which is the natural extension of its counterpart related to axisymmetric, relaxed configurations (Wiegandt1982a-b).

3.2. Rotation parameters

The amount of rotation parameter, h, needed to satisfy Eqs. (28), can be determined via Eqs. (22b) and (23b) by use of Eq. (31). The result is:

$$h = \frac{1}{2}\frac{\nu_{sel}}{\nu_{ram}}\frac{(B_{sel})_{qq}}{(B_{ram})_{qq}}\left[1 - \frac{\zeta_{qq}}{\zeta_{33}}\frac{(B_{sel})_{33}}{(B_{sel})_{qq}}\right] \ ; \quad q = 1, 2 \ ; \tag{33}$$

and the related value of the rotation parameter, $\mathcal{E}_{rot}$, owing to Eqs. (23a) and (33), takes the explicit expression:

$$\mathcal{E}_{rot} = \frac{1}{2}\frac{B_{ram}}{B_{sel}}\frac{(B_{sel})_{qq}}{(B_{ram})_{qq}}\left[1 - \frac{\zeta_{qq}}{\zeta_{33}}\frac{(B_{sel})_{33}}{(B_{sel})_{qq}}\right] \ ; \quad q = 1, 2 \ ; \tag{34}$$

where $\zeta_{qq} = \zeta_{33} = 1/3$ for isotropic, residual velocity distributions (i.e. related to the residual kinetic energy); $\epsilon_{q2} = \epsilon_{q1} = 1$ for spheroidal configurations; $(1+\epsilon_{21}^2)B_{ram} = 1/2$, $\nu_{ram} = 5$, for rigidly rotating configurations; $\nu_{sel} = 3/10$ for homogeneous configurations.

The validity of Eq. (33), or equivalently Eq. (34), implies the following relation:

$$\zeta_{33}\left[(B_{sel})_{11}(B_{ram})_{22} - (B_{sel})_{22}(B_{ram})_{11}\right] = (B_{sel})_{33}\left[\zeta_{11}(B_{ram})_{22} - \zeta_{22}(B_{ram})_{11}\right] \ ; \tag{35}$$

which links the axis ratios, ϵ_{21} and ϵ_{31}, with the anisotropy parameters, ζ_{11} and ζ_{22}, owing to Eq. (26). For fixed values of the (generalized or effective) anisotropy parameters, Eq. (35) describes the change of an axis ratio as a function of the other one, along the related sequence of virial equilibrium configurations.

The rotation parameters, h and $\mathcal{E}_{rot}$, expressed by Eqs. (33) and (34), respectively, exhibit a substantial difference: while the former depends on profile factors, ν_{sel} and ν_{ram}, the latter does not. Then the value of $\mathcal{E}_{rot}$ remains unchanged for homeoidally striated ellipsoids with fixed axis ratios and anisotropy parameters. With regard to h, the special case of Jacobi ellipsoids reads (e.g., Chandrasekhar 1962, but the notation is different therein):

$$h = \frac{3}{50}\frac{(1+\epsilon_{21}^2)^2}{\epsilon_{q1}^2}\left[(B_{sel})_{qq} - (B_{sel})_{33}\right] \ ; \quad q = 1, 2 \ ; \tag{36}$$

and the special case of MacLaurin spheroids corresponds to $\epsilon_{21} = 1$, $(B_{ram})_{qq} = 1/8$, owing to Eq. (22c) and rigid rotation. For further details on MacLaurin spheroids and Jacobi ellipsoids see e.g., Jeans (1929, Chap. VIII); Chandrasekhar (1969, Chaps. 5-6); Caimmi (1996a).

At this stage, let us define the rotation parameter:

$$\upsilon = \frac{\Omega^2}{2\pi G\bar{\rho}} \ ; \tag{37}$$

where $\Omega = \Omega(a_1, 0)$ is the angular velocity at the end of the major equatorial semiaxis, denoted as a_1, and $\bar{\rho}$ is the mean density of the ellipsoid:

$$\bar{\rho} = \frac{3}{4\pi}\frac{M}{a_1 a_2 a_3} \ ; \tag{38}$$

the above definition of the rotation parameter, υ, makes a generalization of some special cases mentioned in the literature (e.g., Jeans 1929, Chap. IX, §232; Chandrasekhar & Leboviz 1962). The combination of Eqs. (20), (23b), (37), and (38) yields:

$$h = \frac{3}{2}\eta_{anm}^2\nu_{anm}^2\frac{(1+\epsilon_{21}^2)^2}{\epsilon_{21}\epsilon_{31}}\upsilon \ ; \tag{39}$$

which links the rotation parameters, h and υ.

The combination of Eqs. (22b), (22c), (33), and (39) allows the explicit expression:

$$\upsilon = \frac{1}{3}\frac{\nu_{sel}}{\eta_{rot}\nu_{rot}}\epsilon_{2q}\epsilon_{3q}(B_{sel})_{qq}\left[1 - \frac{\zeta_{qq}}{\zeta_{33}}\frac{(B_{sel})_{33}}{(B_{sel})_{qq}}\right] \quad ; \quad q = 1, 2 \ ; \tag{40}$$

which, in the special case of rigidly rotating, homogeneous configurations with isotropic peculiar velocity distribution, reduces to a known relation for Jacobi ellipsoids and, with the additional demand of axial symmetry, to a known relation for MacLaurin spheroids (e.g., Jeans 1929, Chap. VIII, §§189-193; Chandrasekhar 1969, Chap. 5, §32, Chap. 6, §39; Caimmi 1996a).

In conclusion, Jacobi ellipsoids and MacLaurin spheroids may be conceived as limiting cases within the class of homeoidally striated ellipsoids under discussion i.e. characterized by rotational or angular velocity distribution expressed by Eqs. (11) or (12), respectively. For this reason, we define homeoidally striated ellipsoids or spheroids of the kind considered, as homeoidally striated Jacobi ellipsoids or MacLaurin spheroids, respectively.

On the other hand, one must keep in mind that Jacobi ellipsoids and MacLaurin spheroids are relaxed configurations i.e. in dynamical equilibrium (e.g., Jeans 1929, Chap. VIII, §§189-193; Chandrasekhar 1969, Chap. 5, §32, Chap. 6, §39), while their homeoidally striated counterparts are unrelaxed configurations i.e. in virial equilibrium but, at least in general, not in dynamical (or hydrostatic) equilibrium (e.g., Tassoul 1978, Chap. 4, Sect. 4.3; Chambat 1994; Caimmi 1996a,b). In addition, homeoidally striated ellipsoids approximate to a first extent self-gravitating fluids, at least in connection with typical values of physical parameters, averaged over the whole volume (e.g., Vandervoort 1980; Vandervoort & Welty 1981; Lai et al. 1993).

3.3. Isotropic and anisotropic configurations

The ratios between anisotropy parameters can be obtained via Eq. (33). The result is:

$$\frac{\zeta_{qq}}{\zeta_{33}} = \frac{(B_{sel})_{qq}}{(B_{sel})_{33}} \left[1 - 2h \frac{\nu_{ram}}{\nu_{sel}} \frac{(B_{ram})_{qq}}{(B_{sel})_{qq}} \right] \quad ; \quad q = 1, 2 \ ; \tag{41}$$

$$\frac{\zeta_{11}}{\zeta_{22}} = \frac{\nu_{sel}(B_{sel})_{11} - 2h\nu_{ram}(B_{ram})_{11}}{\nu_{sel}(B_{sel})_{22} - 2h\nu_{ram}(B_{ram})_{22}} \ ; \tag{42}$$

and the combination of Eqs. (26) and (41) yields:

$$\frac{\zeta_{33}}{\zeta} = \frac{(B_{sel})_{33}}{B_{sel}} \left[1 - 2h \frac{\nu_{ram}}{\nu_{sel}} \frac{B_{ram}}{B_{sel}} \right]^{-1} \ ; \tag{43}$$

which provides an alternative expression to Eqs. (33), (34), and (40), as:

$$h = \frac{1}{2} \frac{\nu_{sel}}{\nu_{ram}} \frac{B_{sel}}{B_{ram}} \left[1 - \frac{\zeta}{\zeta_{33}} \frac{(B_{sel})_{33}}{B_{sel}} \right] \ ; \tag{44}$$

$$\mathcal{E}_{rot} = \frac{1}{2} \left[1 - \frac{\zeta}{\zeta_{33}} \frac{(B_{sel})_{33}}{B_{sel}} \right] \ ; \tag{45}$$

$$\upsilon = \frac{1}{3} \frac{\nu_{sel}}{\eta_{rot}\nu_{rot}} \frac{\epsilon_{21}\epsilon_{31}}{1 + \epsilon_{21}^2} B_{sel} \left[1 - \frac{\zeta}{\zeta_{33}} \frac{(B_{sel})_{33}}{B_{sel}} \right] \ ; \tag{46}$$

where the rotation parameter, h, is expressed as a function of profile parameters, shape parameters, and the effective anisotropy parameter, $\tilde{\zeta}_{33} = \zeta_{33}/\zeta$. In addition, Eqs. (44), (45), and (46), have the same formal expression as in the special case of axisymmetric configurations (e.g., Caimmi 1996b).

The combination of Eqs. (41) and (43) yields:

$$\frac{\zeta_{pp}}{\zeta} = \frac{(B_{sel})_{pp}}{B_{sel}} \left[1 - 2h \frac{\nu_{ram}}{\nu_{sel}} \frac{(B_{ram})_{pp}}{(B_{sel})_{pp}} \right] \left[1 - 2h \frac{\nu_{ram}}{\nu_{sel}} \frac{B_{ram}}{B_{sel}} \right]^{-1} \quad ; \quad p = 1, 2, 3 \ ; \tag{47}$$

in the limiting case of a vanishing rotation, $h \to 0$, Eqs. (47) reduce to:

$$\frac{\zeta_{pp}}{\zeta} = \frac{(B_{sel})_{pp}}{B_{sel}} \quad ; \quad p = 1, 2, 3 \ ; \tag{48}$$

where flattening and/or elongation are owing to anisotropic, residual velocity distribution (i.e. related to the residual kinetic energy) only.

In the special case of isotropic configurations, $\zeta_{pp} = 1/3$, $p = 1, 2, 3$, Eq. (44) reduces to:

$$h_{iso} = \frac{1}{2} \frac{\nu_{sel}}{\nu_{ram}} \frac{B_{sel}}{B_{ram}} \left[1 - 3 \frac{(B_{sel})_{33}}{B_{sel}} \right] \ ; \tag{49}$$

and an equivalent expression may be obtained from Eq. (33). The combination of Eqs. (44), and (49) yields:

$$h = h_{iso} + \frac{1}{2} \frac{\nu_{sel}}{\nu_{ram}} \frac{3\tilde{\zeta}_{33} - 1}{\tilde{\zeta}_{33}} \frac{(B_{sel})_{33}}{B_{ram}} \ ; \tag{50}$$

which shows the effect of polar (with respect to equatorial) anisotropy for a fixed shape.

Values $\tilde{\zeta}_{33} < 1/3$ make $h < h_{iso}$ i.e. less rotation is needed for a fixed flattening, as a contribution from anisotropy arises. The anisotropy parameter cannot be lower than a critical value, which corresponds to $h = 0$; if otherwise, the shape under consideration would not be related to a configuration of virial equilibrium. On the contrary, values $\tilde{\zeta}_{33} > 1/3$ make $h > h_{iso}$ i.e. more rotation is needed for a fixed flattening, as a contribution from anisotropy arises, but in the opposite sense with respect to the former case.

Following a similar procedure, Eq. (46) reads:

$$\upsilon = \upsilon_{iso} + \frac{1}{3}\frac{\nu_{sel}}{\eta_{rot}\nu_{rot}}\frac{\epsilon_{21}\epsilon_{31}}{1+\epsilon_{21}^2}\frac{3\tilde{\zeta}_{33}-1}{\tilde{\zeta}_3}(B_{sel})_{33} \ ; \tag{51a}$$

$$\upsilon_{iso} = \frac{1}{3}\frac{\nu_{sel}}{\eta_{rot}\nu_{rot}}\frac{\epsilon_{21}\epsilon_{31}}{1+\epsilon_{21}^2}\left[B_{sel} - 3(B_{sel})_{33}\right] \ ; \tag{51b}$$

where the effect of anisotropy occurs as discussed above.

Owing to Eqs. (4), (24), and (26), the total energy of a homeoidally striated, Jacobi ellipsoid is:

$$E = \frac{1}{2}E_{sel} + (1-\zeta)E_{res} = -\frac{1}{2}\nu_{sel}\frac{GM^2}{a_1}B_{sel}\left[1 - \frac{1-\zeta}{\zeta}\frac{\zeta}{\zeta_{33}}\frac{(B_{sel})_{33}}{B_{sel}}\right] \ ; \tag{52}$$

and the combination of Eqs. (23b), (33), and (52) yields the explicit expression of the rotation parameter, λ (e.g., Peebles 1969):

$$\lambda^2 = -\frac{J^2E}{G^2M^5} = \frac{1}{4}\frac{\nu_{sel}^2}{\nu_{ram}}\frac{(B_{sel})_{qq}}{(B_{ram})_{qq}}\left[1 - \frac{\zeta_{qq}}{\zeta_{33}}\frac{(B_{sel})_{33}}{(B_{sel})_{qq}}\right]B_{sel}\left[1 - \frac{1-\zeta}{\zeta}\frac{\zeta}{\zeta_{33}}\frac{(B_{sel})_{33}}{B_{sel}}\right] \ ;$$
$$q = 1, 2 \ ; \tag{53}$$

an equivalent expression may be obtained using Eq. (44) instead of (33); the result is:

$$\lambda^2 = \frac{1}{4}\frac{\nu_{sel}^2}{\nu_{ram}}\frac{B_{sel}^2}{B_{ram}}\left[1 - \frac{\zeta}{\zeta_{33}}\frac{(B_{sel})_{33}}{B_{sel}}\right]\left[1 - \frac{1-\zeta}{\zeta}\frac{\zeta}{\zeta_{33}}\frac{(B_{sel})_{33}}{B_{sel}}\right] =$$
$$= \frac{1}{2}\nu_{sel}B_{sel}h\left[1 - \frac{1-\zeta}{\zeta}\frac{\zeta}{\zeta_{33}}\frac{(B_{sel})_{33}}{B_{sel}}\right] \ ; \tag{54}$$

which is a generalization of an expression, previously calculated for homeoidally striated Jacobi ellipsoids, where $\zeta_{11} = \zeta_{22}$ (Caimmi 1993b).

Let us define, using Eq. (30), a typical rms residual velocity, $< v_{res}^2 >= 2E_{res}/M$, as:

$$< v_{res}^2 >= \frac{\nu_{sel}}{\zeta_{33}}\frac{GM}{a_1}(B_{sel})_{33} \ ; \tag{55}$$

and define, using Eqs. (22a) and (31), a typical square rotational velocity, $< v_{rot}^2 >= 2E_{rot}/M$, as:

$$< v_{rot}^2 >= \nu_{sel}\frac{GM}{a_1}\left[B_{sel} - \frac{\zeta}{\zeta_{33}}(B_{sel})_{33}\right] \ ; \tag{56}$$

then the combination of Eqs. (55) and (56) yields:

$$\chi_v^2 = \frac{< v_{rot}^2 >}{< v_{res}^2 >} = \zeta\left[\frac{\zeta_{33}}{\zeta}\frac{B_{sel}}{(B_{sel})_{33}} - 1\right] \ ; \tag{57}$$

which for anisotropic, spheroidal configurations rotating around their symmetry axis, attains a different expression with respect to e.g., Binney & Tremaine (1987, Chap. 4, § 3), owing to a different definition of $< v_{res}^2 >$ therein. The rms velocity ratio, χ_v, may also be considered as a rotation parameter.

However, some caution has to be used in the interpretation of these results. According to Eq. (57) the rms velocity ratio, χ_v, depends only on the axis ratios, ϵ_{21} and ϵ_{31}, and the generalized anisotropy parameter, ζ_{33} (e.g., Binney 1976; Binney & Tremaine 1987, Chap. 4, § 3). Then homeoidally striated ellipsoids with different density profiles and same generalized anisotropy parameter and axis ratios, have the same rms velocity ratio. On the other hand, it is not true for self-gravitating fluids, at least in the limit of isotropic, peculiar velocity distributions, where the rms velocity ratio tends to zero as the density profile tends to the Roche limit,

i.e. a mass point surrounded by a massless atmosphere (Caimmi 1980; 1983). This discrepancy is probably owing to the fact, that (for an assigned generalized anisotropy parameter) the isopycnic surfaces are (taken to be) rotationally distorted at the same extent for homeoidally striated ellipsoids, while rotational distorsion increases passing from the centre to the boundary for self-gravitating fluids.

3.4. Sequences of homeoidally striated Jacobi ellipsoids

Sequences of homeoidally striated Jacobi ellipsoids may be generated using Eqs. (25) and (35), which make a system of three equations involving five unknowns: the effective anisotropy parameters, $\tilde{\zeta}_{pp}$, and the axis ratios, ϵ_{21} and ϵ_{31}. If effective anisotropy parameters are kept constant along the sequence, then Eq. (35) reduces to a relation involving axis ratios only, and the rotation parameter, h, may be determined using Eq. (40). If, on the other hand, the rotation parameter is kept constant along the sequence, then Eqs. (25) and (33) make a system of three equations in five unknowns, and the allowed values of the effective anisotropy parameters, or other rotation parameters, are represented by a surface, $z = z(\epsilon_{21}, \epsilon_{31})$.

In the special case of Jacobi ellipsoids, incompressibility acts as an isotropic, residual velocity distribution and ellipticities are owing to rotation only, and the related sequence is characterized by $\tilde{\zeta}_{pp} = 1/3$, $p = 1, 2, 3$ (e.g., Jeans 1929, Chap. VIII; Chandrasekhar 1966, Chaps. 5-8). It is true also for gaseous, relaxed, homeoidally striated Jacobi ellipsoids, where the collisional nature of the fluid (in absence of systematic motions different from rotation) necessarily yields an isotropic residual velocity distribution, which coincides with Maxwell's distribution (e.g., Jeans 1929, Chap. IX; James 1964). On the contrary, an anisotropic residual velocity distribution may occur in presence of systematic motions different from rotation within collisionless fluids (e.g., Wiegandt 1982 a,b), such as stars or non baryonic dark matter.

Generally speaking, there is no apparent criterion for the selection of a specified sequence of homeoidally striated Jacobi ellipsoids, instead of one other. To this respect, only the nature of the special problem under consideration could provide further information. For this reason, our attention shall be limited to sequences with constant effective anisotropy parameters, $\tilde{\zeta}_{pp}$, starting from a nonrotating, axisymmetric configuration. Accordingly, $\tilde{\zeta}_{11} = \tilde{\zeta}_{22}$, via Eq. (48). The ending point is related to an oblong configuration, unless centrifugal support at the ends of the major equatorial axis occurs earlier.

The equatorial axis ratio, ϵ_{21}, as a function of the polar axis ratio, ϵ_{31}, for sequences of density profiles of the kind considered, is plotted in Fig. 1 with regard to initial, nonrotating ($h = 0$), spheroidal boundaries characterized by polar axis ratios within the range $0.1 \leq (\epsilon_{31})_{h=0} \leq 10$. The bifurcation from axisymmetric to triaxial configurations is marked by a filled circle on each curve. The bifurcation from a round boundary takes place in a sequence where $(\epsilon_{31})_{h=0} = 1.97698$. Each sequence is characterized by the initial, nonrotating boundary, i.e. the effective anisotropy parameters, $\tilde{\zeta}_{pp}$, but it is independent of the special choice of density profile and (systematic rotation) velocity profile.

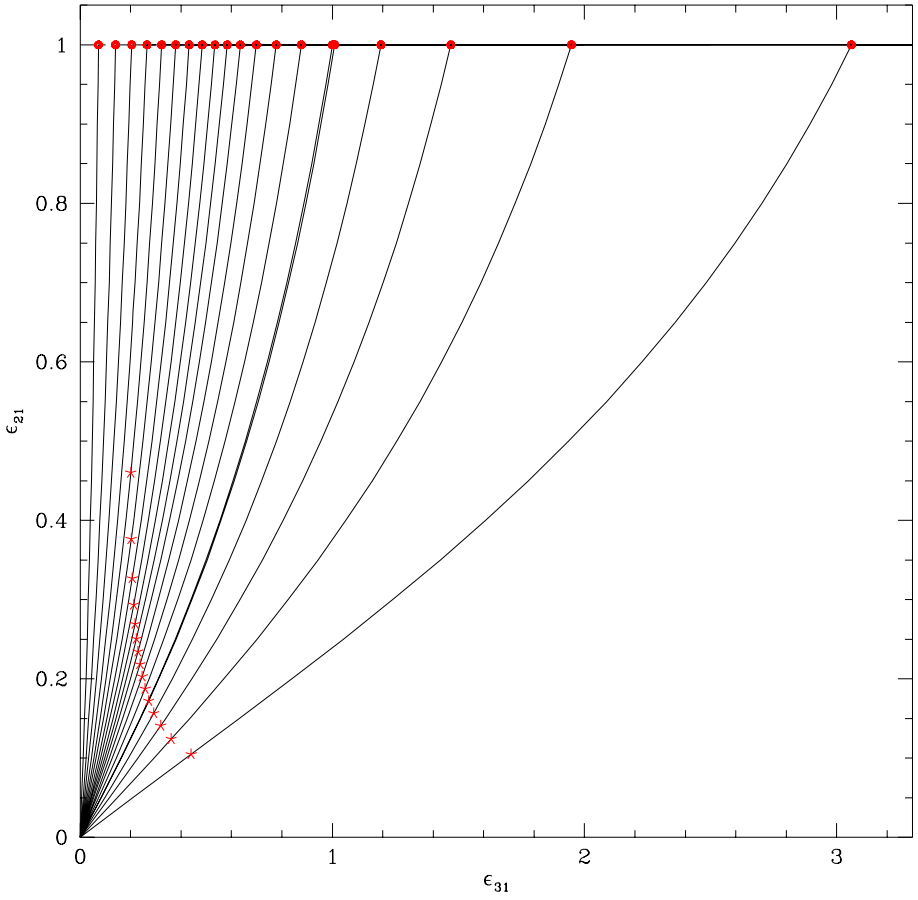

Fig. 1. The equatorial axis ratio, ϵ_{21}, as a function of the polar axis ratio, ϵ_{31}, for sequences of density profiles in virial equilibrium starting from nonrotating ($h = 0$), spheroidal boundaries, with polar axis ratios $(\epsilon_{31})_{h=0} = 0.1\ i$ (oblate) and $(\epsilon_{31})_{h=0} = 1/(0.1\ i)$ (prolate), $1 \leq i \leq 10$. The bifurcation from axisymmetric to triaxial configurations is marked by a filled circle on each curve. The bifurcation from a round boundary takes place in a sequence where $(\epsilon_{31})_{h=0} = 1.97698$. A pentagon skeleton on each curve marks the upper limit of polar axis ratio, for which a necessary condition for the occurrence of centrifugal support at the ends of the equatorial major axis, is first satisfied with regard to a NFW density profile (see Subsect. 4.5) in rigid rotation.

The same holds for the rotation parameter, $\mathcal{E}_{rot}$, defined by Eq. (45). With regard to the remaining rotation parameters, let us define their normalized counterparts, via Eqs. (44), (46), (54), and (57):

$$h_N = \frac{\nu_{ram}}{\nu_{sel}} h = \frac{1}{2} \frac{B_{sel}}{B_{ram}} \left[1 - \frac{\zeta}{\zeta_{33}} \frac{(B_{sel})_{33}}{B_{sel}} \right] \quad ; \tag{58}$$

$$\upsilon_N = \frac{\eta_{rot} \nu_{rot}}{\nu_{sel}} \upsilon = \frac{1}{3} \frac{\epsilon_{21} \epsilon_{31}}{1 + \epsilon_{21}^2} B_{sel} \left[1 - \frac{\zeta}{\zeta_{33}} \frac{(B_{sel})_{33}}{B_{sel}} \right] \quad ; \tag{59}$$

$$\lambda_N^2 = \frac{\nu_{ram}}{\nu_{sel}^2} \frac{\eta_{rot}}{\eta_{anm}^2} \left[1 - \frac{\zeta^{-1} - 1}{1 + \zeta^{-1} \chi_v^2} \right]^{-1} \lambda^2 = \frac{1 + \epsilon_{21}^2}{4} B_{sel}^2 \left[1 - \frac{\zeta}{\zeta_{33}} \frac{(B_{sel})_{33}}{B_{sel}} \right] \quad ; \tag{60}$$

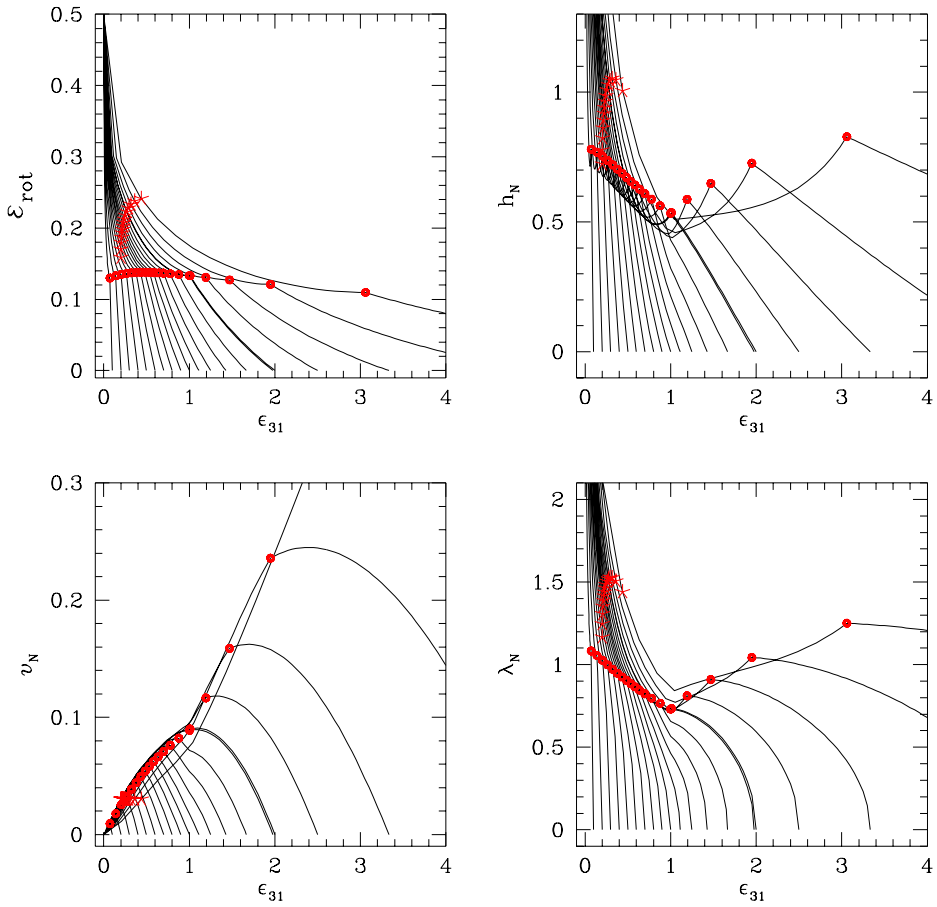

Fig. 2. The rotation parameters, $\mathcal{E}_{rot}$, h_N, λ_N, and υ_N (from top left in clockwise sense), as a function of the polar axis ratio, ϵ_{31}, for sequences of density profiles in virial equilibrium, starting from nonrotating ($h = 0$), spheroidal boundaries, with polar axis ratio $(\epsilon_{31})_{h=0} = 0.1\ i$ (oblate) and $(\epsilon_{31})_{h=0} = 1/(0.1\ i)$ (prolate), $1 \leq i \leq 10$. Other captions as in Fig. 1. All the curves end at the oblong configuration, where the axis ratios tend to zero. The related values of the rotation parameters, $\mathcal{E}_{rot}$ and υ_N, tend to 0.5 and 0, respectively, while h_N and λ_N tend to infinity.

$$\chi_N^2 = \frac{\chi_v{}^2}{\zeta} \ ; \tag{61}$$

which are also independent of both density profile and (systematic rotation) velocity profile.

The rotation parameters, $\mathcal{E}_{rot}$, h_N, λ_N, and υ_N (from top left in clockwise sense), as a function of the axis ratios, ϵ_{31} and ϵ_{21}, are plotted in Figs. 2 and 3, respectively, for sequences of density profiles in virial equilibrium starting from nonrotating ($h = 0$), spheroidal boundaries, with polar axis ratios $(\epsilon_{31})_{h=0} = 0.1\ i$ (oblate) and $(\epsilon_{31})_{h=0} = 1/(0.1\ i)$ (prolate), $1 \leq i \leq 10$. Each curve is characterized by the effective anisotropy parameters, $\tilde{\zeta}_{pp}$, but is independent of both density profile and (systematic rotation) velocity profile.

The rotation parameter, χ_N, as a function of the axis ratios, ϵ_{31} and ϵ_{21}, is plotted in Fig. 4 for sequences of density profiles in virial equilibrium starting from nonrotating ($h =$

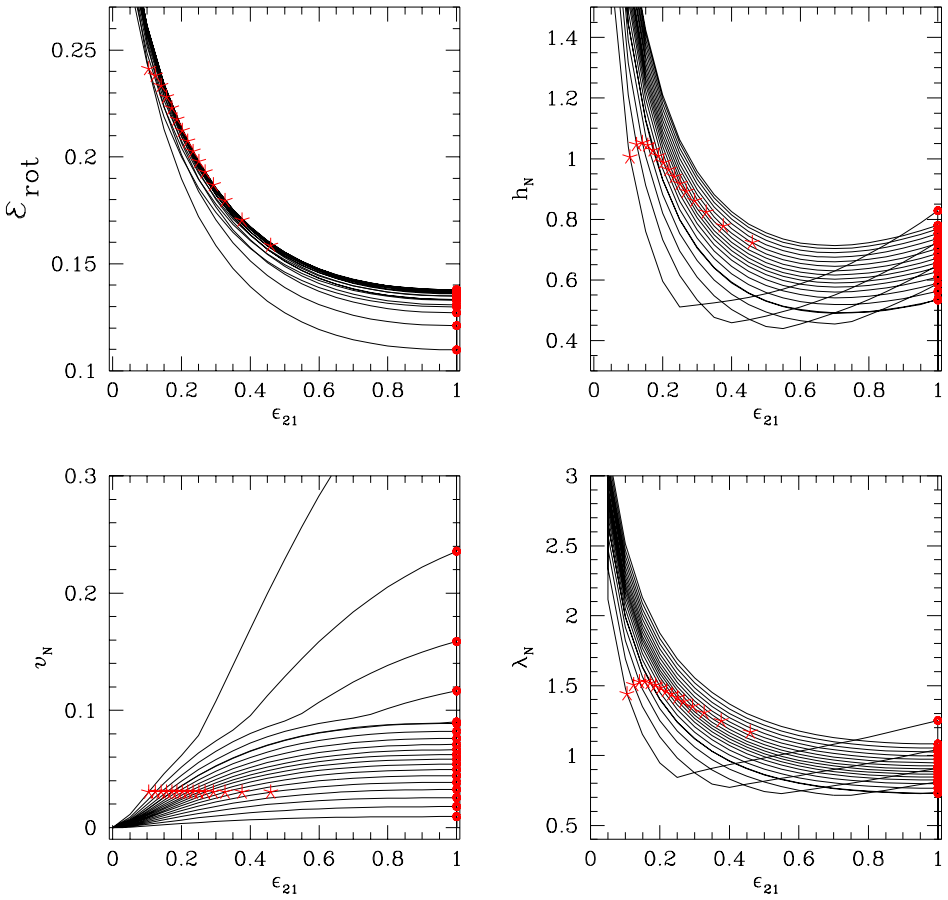

Fig. 3. The rotation parameters, $\mathcal{E}_{rot}$, h_N, λ_N, and υ_N (from top left in clockwise sense), as a function of the equatorial axis ratio, ϵ_{21}, for sequences of density profiles in virial equilibrium, starting from nonrotating ($h = 0$), spheroidal boundaries, with polar axis ratio $(\epsilon_{31})_{h=0} = 0.1\ i$ (oblate) and $(\epsilon_{31})_{h=0} = 1/(0.1\ i)$ (prolate), $1 \leq i \leq 10$. Other captions as in Fig. 1. All the curves end at the oblong configuration, where the axis ratios tend to zero. The related values of the rotation parameters, $\mathcal{E}_{rot}$ and υ_N, tend to 0.5 and 0, respectively, while h_N and λ_N tend to infinity. The coordinates of the nonrotating configurations are (1,0) in each panel.

0), spheroidal boundaries, with polar axis ratios $(\epsilon_{31})_{h=0} = 0.1\ i$ (oblate) and $(\epsilon_{31})_{h=0} = 1/(0.1\ i)$ (prolate), $1 \leq i \leq 10$.

Axis ratios and normalized rotation parameters related to virial equilibrium configurations belonging to three typical sequences, are listed in Tabs. 1, 3, and **??**, where the starting nonrotating configuration is oblate (anisotropy induces flattening), spherical (ispotropic case), and prolate (anisotropy induces elongation), respectively.

3.5. A necessary condition for centrifugal support

With regard to Jacobi ellipsoids, rotational equilibrium i.e. balance between gravitational and centrifugal force, first occurs at the end of the major equatorial semiaxis, for flat or oblong

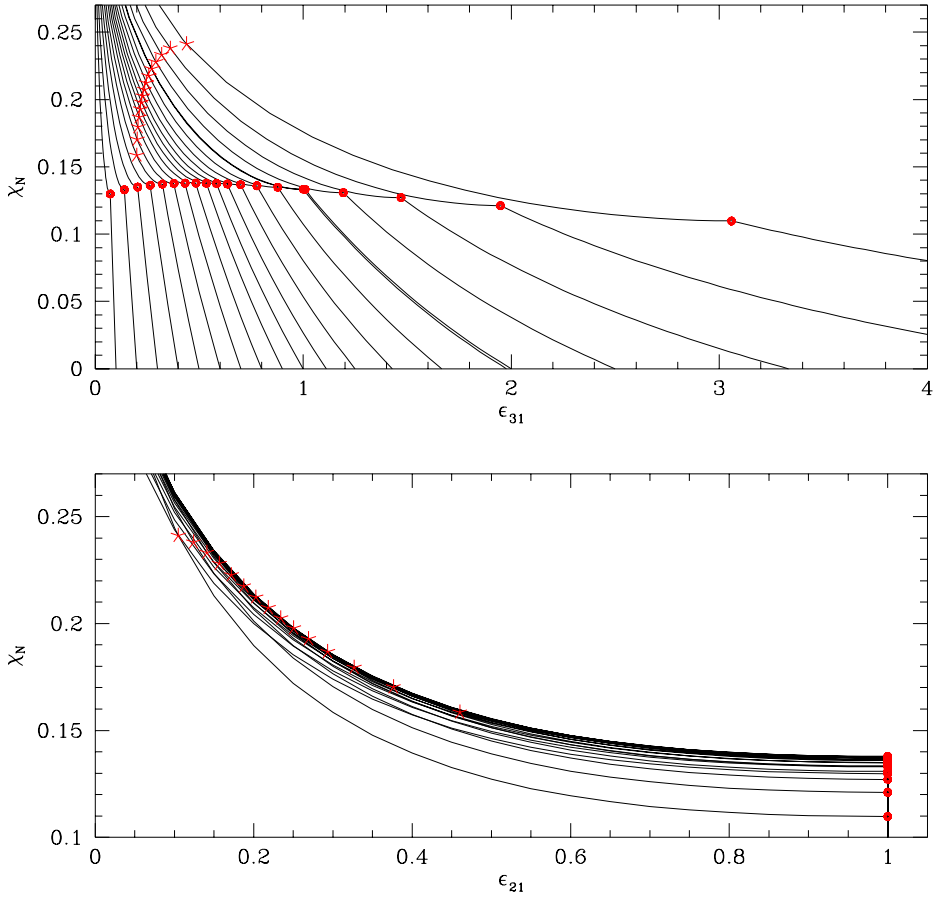

Fig. 4. The rotation parameter, χ_N, as a function of the polar axis ratio, ϵ_{31} (upper panel) and the equatorial axis ratio, ϵ_{21} (lower panel), for sequences of density profiles in virial equilibrium starting from nonrotating ($h = 0$), spheroidal boundaries, with polar axis ratios $(\epsilon_{31})_{h=0} = 0.1\ i$ (oblate) and $(\epsilon_{31})_{h=0} = 1/(0.1\ i)$ (prolate), $1 \leq i \leq 10$. Other captions as in Fig. 1. All the curves end at the oblong configuration, where the axis ratios tend to zero and the rotation parameter, χ_N, tends to infinity. The coordinates of the starting configuration related to all the sequences are $(1, 0)$ in the lower panel.

configurations (e.g., Caimmi 1980). On the other hand, homeoidally striated Jacobi ellipsoids show rotational equilibrium for less flattened or less elongated configurations. The calculation of the gravitational force induced by density profiles of the kind considered, involves numerical integrations (e.g., Chandrasekhar 1969, Chap. 3, §20) and is outside the aim of the current attempt.

Our attention shall be restricted here to two limiting situations, for which the calculation of the gravitational force induced by the mass distribution is simple, and the corresponding range includes the gravitational force induced by the system under investigation. In addition, our considerations will be restricted to the boundary, which is the case of physical interest. On the other hand, the procedure may be extended to a generic, isopycnic surface.

ϵ_{31}	ϵ_{21}	$\mathcal{E}_{rot}$	h_N	υ_N	λ_N	χ_N
0.500000	1.00	0.0000000	0.000000	0.0000000	0.000000	0.000000
0.450000	1.00	0.0355346	0.175722	0.0131792	0.466092	0.276598
0.400000	1.00	0.0733964	0.371350	0.0247567	0.685355	0.414787
0.350000	1.00	0.113834	0.589724	0.0344006	0.873944	0.542936
0.322650	**1.00**	**0.137144**	**0.719984**	**0.0387171**	**0.972086**	**0.614782**
0.314355	0.95	0.137244	0.703109	0.0386747	0.972967	0.615092
0.305580	0.90	0.137567	0.688611	0.0385384	0.975802	0.616090
0.296287	0.85	0.138149	0.676710	0.0382934	0.980919	0.617888
0.286432	0.80	0.139034	0.667680	0.0379229	0.988715	0.620622
0.275970	0.75	0.140272	0.661862	0.0374076	0.999672	0.624450
0.264850	0.70	0.141925	0.659686	0.0367259	1.01438	0.629567
0.253015	0.65	0.144066	0.661701	0.0358531	1.03357	0.636204
0.240404	0.60	0.146785	0.668618	0.0347618	1.05816	0.644647
0.226950	0.55	0.150191	0.681374	0.0334219	1.08933	0.655249
0.212577	0.50	0.154418	0.701221	0.0318002	1.12859	0.668457
0.197205	0.45	0.159634	0.729873	0.0298619	1.17795	0.684842
0.180748	0.40	0.166054	0.769728	0.0275717	1.24013	0.705158
0.163111	0.35	0.173953	0.824243	0.0248968	1.31896	0.730426
0.144198	0.30	0.183700	0.898594	0.0218121	1.41997	0.762088
0.123907	0.25	0.195803	1.00092	0.0183099	1.55171	0.802290
0.102147	0.20	0.211000	1.14492	0.0144169	1.72824	0.854462
0.0788405	0.15	0.230466	1.35619	0.0102269	1.97547	0.924692
0.0539566	0.10	0.256360	1.69132	0.00596398	2.35031	1.02577
0.0275656	0.05	0.294098	2.32663	0.00212718	3.02987	1.19513
0.0000000	0.00	0.500000	$+\infty$	0.00000000	$+\infty$	$+\infty$

Table 1. Values of axis ratios, ϵ_{31} and ϵ_{21}, and normalized rotation parameters, $\mathcal{E}_{rot}$, h_N, υ_N, λ_N, χ_N, related to a sequence of virial equilibrium configurations with anisotropy parameters, $\tilde{\zeta}_{11} = \tilde{\zeta}_{22} = 0.391002$ and $\tilde{\zeta}_{33} = 0.217996$. The polar axis ratio of the initial nonrotating configuration is $\epsilon_{31} = 1/2$. Values at the bifurcation point are listed on the boldface line.

Given a homeoidally striated, Jacobi ellipsoid, let us define a related, striated sphere and focaloidally striated ellipsoid, as matter distributions with same scaled density profile, total mass, major equatorial semiaxis and, in the latter case, same boundary. Owing to MacLaurin's theorem (e.g., Chandrasekhar 1969, Chap. 3, §19), the gravitational force induced by the striated sphere and the focaloidally striated ellipsoid at the end of the major equatorial semiaxis, is:

$$F_G(a_1, 0, 0) = -2\pi G\bar{\rho}_w (A_1)_w a_1 \ ; \tag{62}$$

where $\bar{\rho}$ is the mean density, A_1 is a shape factor in the range $0 \leq A_1 \leq 2/3$ with the upper limit related to spherical configurations, and $w = sph, foc,$ for the striated sphere and the focaloidally striated ellipsoid, respectively.

The balance between gravitational and centrifugal force at the end of the major equatorial semiaxis, reads:

$$-2\pi G\bar{\rho}_w(A_1)_w a_1 + \Omega^2 a_1 = 0 \ ; \tag{63}$$

which, using Eq. (37), may be cast under the equivalent form:

$$(\upsilon_{eq})_w = \frac{\Omega^2}{2\pi G\bar{\rho}_w} = (A_1)_w \ ; \tag{64}$$

where the index, eq, denotes the rotation parameter, υ, related to rotational equilibrium at the end of major equatorial semiaxis. The above results allow the validity of the relation:

$$(\upsilon_{eq})_{foc} \leq \upsilon_{eq} \leq (\upsilon_{eq})_{sph} \ ; \tag{65}$$

where υ_{eq} is the critical value related to the homeoidally striated, Jacobi ellipsoid. Then $\upsilon \geq (\upsilon_{eq})_{foc}$ and $\upsilon \leq (\upsilon_{eq})_{sph}$ make a sufficient and a necessary condition, respectively, for the occurrence of rotational equilibrium at the end of major equatorial semiaxis, in homeoidally striated, Jacobi ellipsoids.

Owing to MacLaurin's theorem, the condition of rotational equilibrium, Eq. (64), for focaloidally striated ellipsoids coincides with its counterpart related to homogeneous ellipsoids with equal mean density, axis ratios, and velocity field. On the other hand, the rotation parameter, υ, in the special case of focaloidally striated ellipsoids, is also expressed by Eq. (40), particularized to Jacobi ellipsoids, owing to MacLaurin's theorem. A comparison with Eq. (64) shows that rotational equilibrium in focaloidally striated ellipsoids occurs only for flat configurations, $\epsilon_{31} = 0$. Accordingly, Eq. (65) reduces to:

$$0 \leq \upsilon_{eq} \leq \frac{2}{3} \ ; \tag{66}$$

owing to Eq. (64) and $(A_1)_{sph} = 2/3$, as reported in Appendix B.

4. Transitions from and towards homeoidally striated density profiles

As an application of the results of Sect. 3, let us take into consideration the transition from an initial configuration, with assigned mass, angular momentum, and different kinds of energy, towards a final configuration with assigned mass, angular momentum, and different kinds of energy tensors. Let both initial and final configurations be homeoidally striated ellipsoids, with assigned density profile and rotational velocity profile of the kind discussed in Sect. 2. The above mentioned assumption is only for sake of simplicity. It is worth emphasizing that the procedure outlined in this Section, well holds for any density profile with triplanar symmetry, i.e. symmetric with respect to the principal planes.

The original method conceived by Thuan & Gott (1975) is aimed to be generalized on many respects, namely (i) from spheroidal to ellipsoidal configurations; (ii) from isotropic to anisotropic, residual velocity distributions; (iii) from relaxed to unrelaxed, final configurations; and, in the limit of axisymmetric configurations (iv) from rigid to differential rotation.

In the following, first the general case shall be dealt with, in connection with the transitions of the kind considered, and then a few interesting special cases will be analysed.

4.1. The general case

The investigation of unrelaxed configurations, for which virial equilibrium does not coincide with dynamical (or hydrostatic) equilibrium, goes beyond a purely academic interest. For instance, (non interacting) galaxies and cluster of galaxies (where galaxies are still falling in from outer regions) make examples of (approximately) relaxed and unrelaxed configurations, respectively.

In general, the tensor components, $\tilde{\zeta}_{pp} = \zeta_{pp}/\zeta$ and $(\tilde{E}_{res})_{pq}$, which appear in Eq. (26), have to be considered as effective, instead of actual, anisotropy parameters and residual kinetic-energy tensor, respectively. Then the coincidence of virial equilibrium with dynamical (or hydrostatic) equilibrium is restricted to the special choice $\zeta = 1$ which, on the other hand, makes a necessary condition only. It is worth recalling that the residual kinetic energy, E_{res}, has to be intended as related to all motions different from systematic rotation around a fixed axis, such as random motions, streaming flows, coherent oscillations, and so on. With regard to the initial configuration, the residual kinetic energy will be expressed as the sum of two contributions: one, owing to systematic motions (mainly radial expansion), and one other, owing to random motions.

For sake of brevity, let us define the tensors, together with the related scalar quantities:

$$\mathcal{S}_{pq} = \nu_{sel}(B_{sel})_{pq} \ ; \quad \mathcal{S} = \nu_{sel}B_{sel} \ ; \tag{67}$$

$$\mathcal{R}_{pq} = \nu_{ram}(B_{ram})_{pq} \ ; \quad \mathcal{R} = \nu_{ram}B_{ram} \ ; \tag{68}$$

and let a prime, and its absence, denote the initial and the final configuration, respectively. The effective anisotropy parameters, $\tilde{\zeta}_{pp}$, expressed by Eqs. (47), and the rotation parameters, h, $\mathcal{E}_{rot}$, υ, λ, and χ_v, expressed by Eqs. (44), (45), (46), (54), and (57), respectively, are written in compact notation in Appendix C, using Eqs. (67) and (68).

Owing to Eqs. (4), (22), (67), and (68), the self-potential and rotational energy related to the final and initial configuration, respectively, are:

$$E_{sel} = -\frac{GM^2}{a_1}\mathcal{S} \ ; \quad E'_{sel} = -\frac{GM'^2}{a'_1}\mathcal{S}' \ ; \tag{69}$$

$$E_{rot} = \frac{J^2}{Ma_1^2}\mathcal{R} \ ; \quad E'_{rot} = \frac{J'^2}{M'a_1'^2}\mathcal{R}' \ ; \tag{70}$$

and the identity:

$$E_{rot} = \frac{E_{rot}}{E'_{rot}}\frac{E'_{rot}}{-E'_{sel}}\frac{E'_{sel}}{E_{sel}}(-E_{sel}) \ ;$$

owing to Eqs. (23), (69), and (70), may be cast under the equivalent form:

$$\frac{a'_1}{a_1} = \frac{\beta_M^3}{\beta_J^2}\frac{\mathcal{S}}{\mathcal{S}'}\frac{\mathcal{R}'}{\mathcal{R}}\frac{\mathcal{E}_{rot}}{\mathcal{E}'_{rot}} \ ; \tag{71a}$$

$$\beta_J = \frac{J}{J'} \ ; \quad \beta_M = \frac{M}{M'} \ ; \tag{71b}$$

involving dimensionless quantities only.

On the other hand, the identity:

$$E = E_{sel} + E_{rot} + E_{res} = \frac{E}{E'}E' = \frac{E}{E'}(E'_{sel} + E'_{rot} + E'_{pec} + E'_{osc}) \ ;$$

by use of Eqs. (24), and (26), may be cast under the form:

$$\frac{E_{sel}}{E'_{sel}} - \mathcal{E}_{rot}\frac{E_{sel}}{E'_{sel}} - \frac{1}{2\zeta}\frac{E_{sel}}{E'_{sel}} + \frac{1}{\zeta}\frac{E_{sel}}{E'_{sel}}\mathcal{E}_{rot} = \beta_E(1 - \mathcal{E}'_{rot} - \mathcal{E}'_{pec} - \mathcal{E}'_{osc}) \ ; \tag{72a}$$

$$\beta_E = \frac{E}{E'} \ ; \quad \mathcal{E}_{rot} = -\frac{E_{rot}}{E_{sel}} \ ; \quad \mathcal{E}_{pec} = -\frac{E_{pec}}{E_{sel}} \ ; \quad \mathcal{E}_{osc} = -\frac{E_{osc}}{E_{sel}} \ ; \tag{72b}$$

$$\zeta = -\frac{E_{sel} + 2E_{rot}}{2(E_{osc} + E_{pec})} \ ; \tag{72c}$$

where E_{osc}, E_{pec}, represent the kinetic energy of systematic radial and non systematic motions, respectively. The combination of Eqs. (69), (70), and (72) yields after some algebra:

$$\beta_M^2 \frac{\mathcal{S}}{\mathcal{S}'}\frac{a'_1}{a_1}\left[\frac{2\zeta - 1}{2\zeta} - \frac{\zeta - 1}{\zeta}\mathcal{E}_{rot}\right] - \beta_E(1 - \mathcal{E}'_{rot} - \mathcal{E}'_{pec} - \mathcal{E}'_{osc}) = 0 \ ; \tag{73}$$

involving dimensionless quantities only.

The combination of Eqs. (34), (67), (68), (69), and (70) yields after some algebra:

$$\mathcal{E}_{rot} = \frac{\mathcal{R}}{\mathcal{S}}h = \frac{1}{2}\frac{\mathcal{R}}{\mathcal{S}}\frac{\mathcal{S}_{qq}}{\mathcal{R}_{qq}}\left[1 - \frac{\zeta_{qq}}{\zeta_{33}}\frac{\mathcal{S}_{33}}{\mathcal{S}_{qq}}\right] \ ; \quad q = 1, 2 \ ; \tag{74}$$

which, owing to Eq. (45), is equivalent to:

$$\mathcal{E}_{rot} = \frac{1}{2}\left[1 - \frac{\zeta}{\zeta_{33}}\frac{\mathcal{S}_{33}}{\mathcal{S}}\right] \ ; \tag{75}$$

and Eq. (35) may be written under the equivalent form:

$$\zeta_{33}\left[\mathcal{S}_{11}\mathcal{R}_{22} - \mathcal{S}_{22}\mathcal{R}_{11}\right] = \mathcal{S}_{33}\left[\zeta_{11}\mathcal{R}_{22} - \zeta_{22}\mathcal{R}_{11}\right] \ ; \tag{76}$$

where Eqs. (67) and (68) have also been used. The substitution of Eq. (71a) into (73) produces a second-degree equation in $\mathcal{E}'_{rot}$, as:

$$\mathcal{E}'^2_{rot} - 2b\mathcal{E}'_{rot} + c = 0 \ ; \tag{77a}$$

$$b = \frac{1}{2}\left(1 - \mathcal{E}'_{osc} - \mathcal{E}'_{pec}\right) \ ; \tag{77b}$$

$$c = \frac{\beta_M^5}{\beta_J^2\beta_E}\left(\frac{\mathcal{S}}{\mathcal{S}'}\right)^2\frac{\mathcal{R}'}{\mathcal{R}}\mathcal{E}_{rot}\left[\frac{2\zeta - 1}{2\zeta} - \frac{\zeta - 1}{\zeta}\mathcal{E}_{rot}\right] \ ; \tag{77c}$$

the (reduced) discriminant of this equation is:

$$\Delta = b^2 - \frac{\beta_M^5}{\beta_J^2\beta_E}\left(\frac{\mathcal{S}}{\mathcal{S}'}\right)^2\frac{\mathcal{R}'}{\mathcal{R}}\mathcal{E}_{rot}\left[\frac{2\zeta - 1}{2\zeta} - \frac{\zeta - 1}{\zeta}\mathcal{E}_{rot}\right] \ ; \tag{78}$$

with regard to a transition from an initial to a final configuration, where all the parameters which appear in Eq. (78) are specified, except the axis ratios, ϵ_{21} and ϵ_{31}, the condition $\Delta = 0$ represents, via Eq. (78), a curve in the $(\mathsf{O}\epsilon_{21}\epsilon_{31})$ plane. The transition is forbidden for all values of the axis ratios, which make a negative discriminant, and then imaginary solutions.

The solutions of Eq. (77a) are:

$$\mathcal{E}'_{rot} = b \mp \left\{b^2 - \frac{\beta_M^5}{\beta_J^2\beta_E}\left(\frac{\mathcal{S}}{\mathcal{S}'}\right)^2\frac{\mathcal{R}'}{\mathcal{R}}\mathcal{E}_{rot}\left[\frac{2\zeta - 1}{2\zeta} - \frac{\zeta - 1}{\zeta}\mathcal{E}_{rot}\right]\right\}^{1/2} \ ; \tag{79}$$

and the combination of Eqs. (71a) and (79) yields:

$$\frac{a_1}{a'_1} = \frac{\beta_J^2}{\beta_M^3}\frac{\mathcal{S}'}{\mathcal{S}}\frac{\mathcal{R}}{\mathcal{R}'}\frac{1}{\mathcal{E}_{rot}}\left\{b \mp \left[b^2 - \frac{\beta_M^5}{\beta_J^2\beta_E}\left(\frac{\mathcal{S}}{\mathcal{S}'}\right)^2\frac{\mathcal{R}'}{\mathcal{R}}\mathcal{E}_{rot}\left(\frac{2\zeta - 1}{2\zeta} - \frac{\zeta - 1}{\zeta}\mathcal{E}_{rot}\right)\right]^{1/2}\right\} \ ; \tag{80}$$

where the upper and lower sign correspond to the upper and lower sign in Eq. (79). It is worth noticing that the rotation parameter, $\mathcal{E}'_{rot}$, and the axis ratio, a_1/a'_1, are left unchanged for different departures from mass, angular momentum, and energy conservation, provided the ratios:

$$\beta_{\mathcal{E}} = \frac{\beta_M^5}{\beta_J^2 \beta_E} \ ; \qquad \beta_a = \frac{\beta_J^2}{\beta_M^3} \ ; \tag{81}$$

do not vary.

The explicit expression of Eq. (76) defines a curve in the $(\mathrm{O}\epsilon_{21}\epsilon_{31})$ plane, where the axis ratios of the final configuration must necessarily lie. The intersection between the curves, represented by Eqs. (76) and (78), yields a point where the axis ratios of the limiting, final configuration lies, related to a null discriminant. Final configurations with axis ratios, related to a negative discriminant, cannot occur.

4.2. The limiting case $c \to 0$

The limiting case $c \to 0$, via Eqs. (77), corresponds to $\mathcal{E}'_{rot} = 0$ i.e. nonrotating initial configurations, and to $\mathcal{E}'_{rot} = 2b = 1 - \mathcal{E}'_{osc} - \mathcal{E}'_{pec}$, i.e. unbound configurations. Further inspection to Eq. (77c) discloses that the right hand-side member may tend to zero in a twofold manner, through either the ratio $\mathcal{E}_{rot}/\beta_J^2$ or the difference within square brakets.

With regard to the former alternative, the combination of Eqs. (23b), (71b), and (74) yields:

$$\frac{\mathcal{E}_{rot}}{\beta_J^2} = \frac{\mathcal{R}}{\mathcal{S}} \frac{(J')^2}{GM^3 a_1} \ ; \tag{82}$$

which tends to zero for nonrotating initial configurations and/or infinitely extended final configurations.

With regard to the latter alternative, the difference within square brakets in Eq. (77c) tends to zero provided the rotation parameter, $\mathcal{E}_{rot}$, tends to the value:

$$\mathcal{E}_{rot} = \frac{1}{2} \frac{1-2\zeta}{1-\zeta} \ ; \qquad 0 \leq \zeta \leq \frac{1}{2} \ ; \tag{83}$$

where the condition on the virial index, ζ, is necessary to avoid negative values of the rotation parameter in the case under discussion. The combination of Eqs. (24), (26), and (83) yields a second-degree equation involving $\mathcal{E}_{rot}$ as unknown and $\mathcal{E}_{res}$ as parameter, where $\mathcal{E}_{res} = \mathcal{E}_{osc} + \mathcal{E}_{pec}$ in the case under discussion. The solutions of the above mentioned equation are:

$$\mathcal{E}_{rot} = \frac{1}{4} \ ; \qquad \mathcal{E}_{rot} = \frac{1}{2} - \mathcal{E}_{res} \ ; \tag{84}$$

and the substitution into Eq. (83) yields:

$$\zeta = \frac{1}{3} \ ; \qquad \zeta = \frac{2\mathcal{E}_{res}}{1 + 2\mathcal{E}_{res}} \ ; \tag{85}$$

where the former solution, via Eqs. (24) and (26), corresponds to $\mathcal{E}_{res} = 3/4$, and then to an unbound i.e. infinitely extended final configuration, as $\mathcal{E}_{rot} + \mathcal{E}_{res} = 1$. On the other hand, the latter solution clearly represents a relaxed configuration, as $\mathcal{E}_{rot} + \mathcal{E}_{res} = 0.5$, which would necessarily imply $\zeta = 1$, contrary to what has been found. Then the limiting case $c \to 0$ is attained by making the ratio $\mathcal{E}_{rot}/\beta_J^2$ tend to zero.

4.3. Virialized, final configurations

In the special case of relaxed, final configurations, $\zeta = 1$, virial equilibrium coincides with dynamical (or hydrostatic) equilibrium. Accordingly, Eq. (77c) translates into:

$$c = \frac{1}{2}\frac{\beta_M^5}{\beta_J^2\beta_E}\left(\frac{\mathcal{S}}{\mathcal{S}'}\right)^2\frac{\mathcal{R}'}{\mathcal{R}}\mathcal{E}_{rot} \ ; \tag{86}$$

similarly, Eqs. (79) and (80) reduce to:

$$\mathcal{E}'_{rot} = b \mp \left[b^2 - \frac{1}{2}\frac{\beta_M^5}{\beta_J^2\beta_E}\left(\frac{\mathcal{S}}{\mathcal{S}'}\right)^2\frac{\mathcal{R}'}{\mathcal{R}}\mathcal{E}_{rot}\right]^{1/2} \ ; \tag{87}$$

$$\frac{a_1}{a'_1} = \frac{\beta_J^2}{\beta_M^3}\frac{\mathcal{S}'}{\mathcal{S}}\frac{\mathcal{R}}{\mathcal{R}'}\frac{1}{\mathcal{E}_{rot}}\left\{b \mp \left[b^2 - \frac{1}{2}\frac{\beta_M^5}{\beta_J^2\beta_E}\left(\frac{\mathcal{S}}{\mathcal{S}'}\right)^2\frac{\mathcal{R}'}{\mathcal{R}}\mathcal{E}_{rot}\right]^{1/2}\right\} \ ; \tag{88}$$

where the upper and lower sign must correspond in both equations.

4.4. Nonrotating, initial configurations

In the special case of initial configurations with vanishing angular momentum, $J' \to 0$, the parameter, β_J^{-1}, has necessarily to remain finite. Accordingly, the combination of Eqs. (23b), (71b), and (74) yields:

$$\beta_J^2\mathcal{E}'_{rot} = \frac{\mathcal{R}'}{\mathcal{S}'}\frac{J^2}{G(M')^3 a'_1} \ ; \tag{89}$$

$$\beta_J^2(\mathcal{E}'_{rot})^2 = \left(\frac{\mathcal{R}'}{\mathcal{S}'}\right)^2\frac{J^2(J')^2}{G^2(M')^6(a'_1)^2} \ ; \tag{90}$$

where the product on the left-hand side of Eq. (90) is infinitesimal of higher order with respect to its counterpart related to Eq. (89). Then Eq. (77a) reduces to a first-degree equation, and Eqs. (79) and (80) reduce to:

$$\beta_J^2\mathcal{E}'_{rot} = \frac{1}{2}\frac{\beta_M^5}{\beta_E}\left(\frac{\mathcal{S}}{\mathcal{S}'}\right)^2\frac{\mathcal{R}'}{\mathcal{R}}\mathcal{E}_{rot}\left[\frac{2\zeta-1}{2\zeta} - \frac{\zeta-1}{\zeta}\mathcal{E}_{rot}\right]\frac{1}{b} \ ; \tag{91}$$

$$\frac{a_1}{a'_1} = \frac{1}{2}\frac{\beta_M^2}{\beta_E}\frac{\mathcal{S}}{\mathcal{S}'}\left[\frac{2\zeta-1}{2\zeta} - \frac{\zeta-1}{\zeta}\mathcal{E}_{rot}\right]\frac{1}{b} \ ; \tag{92}$$

respectively. It is worth noticing that unbound configurations correspond to $b = 0$, via Eqs. (72b) and (77b).

If, in addition, the rotation energy of the final configuration is negligible in respect of the self-potential energy, $\mathcal{E}_{rot} \to 0$, Eqs. (91) and (92) reduce to:

$$\beta_J^2\mathcal{E}'_{rot} = \frac{1}{2}\frac{\beta_M^5}{\beta_E}\left(\frac{\mathcal{S}}{\mathcal{S}'}\right)^2\frac{\mathcal{R}'}{\mathcal{R}}\mathcal{E}_{rot}\frac{2\zeta-1}{2\zeta}\frac{1}{b} \ ; \tag{93}$$

$$\frac{a_1}{a'_1} = \frac{1}{2}\frac{\beta_M^2}{\beta_E}\frac{\mathcal{S}}{\mathcal{S}'}\frac{2\zeta-1}{2\zeta}\frac{1}{b} \ ; \tag{94}$$

where both sides of Eq. (93) have necessarily to be infinitesimal of the same order.

In the special case of a relaxed, final configuration, which necessarily implies $\zeta = 1$ according to Eqs. (24) and (26), Eqs. (87) and (88) reduce to Eqs. (91) and (92), respectively, particularized to the special case, $\zeta = 1$. The result is:

$$\beta_J^2\mathcal{E}'_{rot} = \frac{1}{4}\frac{\beta_M^5}{\beta_E}\left(\frac{\mathcal{S}}{\mathcal{S}'}\right)^2\frac{\mathcal{R}'}{\mathcal{R}}\mathcal{E}_{rot}\frac{1}{b} \ ; \tag{95}$$

$$\frac{a_1}{a'_1} = \frac{1}{4}\frac{\beta_M^2}{\beta_E}\frac{\mathcal{S}}{\mathcal{S}'}\frac{1}{b} \ ; \tag{96}$$

where the trend is the same as shown above.

4.5. Application to dark matter haloes

Dark matter haloes make a natural application of the procedure outlined above, as they are the counterpart of elliptical galaxies passing from baryonic to dark matter universes. Aiming to see nothing but the method at work, our attention shall be restricted here to (i) CDM cosmological models and (ii) (non baryonic) dark matter, which is equivalent to assume a homeoidally striated density profile also for baryonic matter where, in addition, the isopycnic surfaces are similar and similarly placed with respect to the boundary (e.g., CM03).

The current procedure has a main advantage on numerical simulations, that the initial configuration may be taken as an overdensity region at recombination epoch. In this case, the dominant energies are expected to be the potential and the kinetic one, the latter related to systematic, expansion motions, and the mass distribution may safely be thought of as a homogeneous sphere. Computations usually start much later, owing to their high cost and time machine. The choice of recombination epoch as starting time makes the initial configuration virtually independent of the cosmological model, at least for sufficiently large, present-day density parameters ($\Omega_0 \geq 0.1$), where the related universe may be considered flat to a good extent i.e. $|1 - \Omega_{rec}^{-1}| \ll 1$ (e.g., Zeldovich & Novikov 1982, Chap. III, §4; Caimmi & Marmo 2004).

Let us represent overdense regions as made of two subsystems with coinciding volume, namely (i) the unperturbed, cosmological fluid, with density equal to the mean density of the universe, ρ_h, and (ii) the density perturbation, with mean density equal to the difference between the overdensity and the mean density of the universe, $\delta\bar{\rho} = \bar{\rho} - \rho_h$. At recombination epoch, overdense regions may safely be thought of as homogeneous and spherical. This is why the overdensity index, $\bar{\delta}_{rec} = \delta\bar{\rho}/\rho_h$, cannot exceed (in absolute value) a few percents at that time (e.g., Gunn 1987). In addition, tidal distorsions from sphericity are owing to neighbouring density perturbations, while tidal distorsions towards sphericity are owing to the unperturbed, cosmological fluid.

In general, the potential-energy tensor of an overdensity region is the sum of three contributions, namely: (i) the self-energy tensor of the overdense region, (ii) the tidal-energy tensor induced by the unperturbed, cosmological fluid outside the overdense region, and (iii) the tidal-energy tensor induced by neighbouring density perturbations. For reasons mentioned above, the last two contributions may safely be neglected in the case under discussion. Accordingly, the combination of Eqs. (4), (5), and (67); (22) and (68); yields:

$$\mathcal{S}'_{pq} = \frac{1}{5}\delta_{pq} \ ; \quad \mathcal{S}' = \frac{3}{5} \ ; \tag{97}$$

$$\mathcal{R}'_{pq} = \frac{5}{8}\delta_{pq}(1 - \delta_{p3}) \ ; \quad \mathcal{R}' = \frac{5}{4} \ ; \tag{98}$$

respectively, as $\nu_{sel} = 3/10$ and $A_1 = A_2 = A_3 = 2/3$ in the case under discussion of a homogeneous sphere; and $\eta_{anm} = 2\eta_{rot} = 1$, $\nu_{anm} = \nu_{rot} = \nu_{inr} = 1/5$ for a homogeneous, rigidly rotating sphere.

The kinetic-energy tensor of systematic, expansion motions, is:

$$(E'_{osc})_{pq} = \frac{1}{10}\delta_{pq}M'\dot{a}'^2 \ ; \quad E'_{osc} = \frac{3}{10}M'\dot{a}'^2 \ ; \tag{99}$$

in the case under discussion of a homogeneous sphere. The further assumption that, at recombination epoch, the overdense region expands at the same rate as the unperturbed, cosmological fluid, implies the validity of the relation:

$$\dot{a}' = (\dot{a}_h)_{rec} = H_{rec}(a_h)_{rec} = H_{rec}a' \ ; \tag{100}$$

where a_h is the scale factor of the universe, H is the Hubble parameter, and the index rec denotes the recombination epoch.

At sufficiently early times i.e. high redshifts, in particular at the recombination epoch ($z_{rec} \sim 1400$), the following relations hold (e.g., Zeldovich & Novikov 1982, Chap. III, §4):

$$\Omega^{-1}(z) = 1 + \frac{1}{1+z}\frac{1-\Omega_0}{\Omega_0} \ ; \quad \Omega_0 \geq 0.1 \ ; \tag{101}$$

$$\rho_h(z) = \frac{3}{8\pi}\frac{H_0^2}{G}(1+z)^3 \ ; \quad |1-\Omega^{-1}| \ll 1 \ ; \tag{102}$$

$$H(z) = \frac{2}{3}\frac{1}{t} = H_0(1+z)^{3/2} \ ; \quad |1-\Omega^{-1}| \ll 1 \ ; \tag{103}$$

where Ω is the density parameter (to be not confused with the angular velocity), z the redshift, t the time, and the index 0 denotes the present-day epoch. The definition of the density parameter reads:

$$\Omega = \frac{\rho_h}{(\rho_h)_{crit}} \ ; \qquad (\rho_h)_{crit} = \frac{3H^2}{8\pi G} \ ; \tag{104}$$

where $(\rho_h)_{crit}$ is the critical density i.e. the density of the Hubble flow in an Einstein-de Sitter universe.

By use of the definition of mean density inside an overdense region, $\bar{\rho} = \rho_h + \delta\bar{\rho} = \rho_h(1+\bar{\delta}) = 3M_h(1+\bar{\delta})/(4\pi a_h^3)$, and Eqs. (100), (102), and (103), the following relations are derived after some algebra:

$$a' = \left[\frac{2GM'}{H_0^2(1+\bar{\delta}_{rec})}\right]^{1/3}\frac{1}{1+z_{rec}} \ ; \tag{105}$$

$$\dot{a}' = H_0(1+z_{rec})^{3/2}a' = \left(\frac{2GM'H_0}{1+\bar{\delta}_{rec}}\right)^{1/3}(1+z_{rec})^{1/2} \ ; \tag{106}$$

and the combination of Eqs. (99) and (100) reads:

$$(E'_{osc})_{pq} = \frac{1}{10}\delta_{pq}H_{rec}^2M'a'^2 \ ; \quad E'_{osc} = \frac{3}{10}H_{rec}^2M'a'^2 \ ; \tag{107}$$

in the case under consideration of a homogeneous sphere expanding at the same rate as the universe. The combination of Eqs. (67), (69), (72b), (104) and (107) yields:

$$\mathcal{E}'_{osc} = \left[\Omega_{rec}(1+\bar{\delta}_{rec})\right]^{-1} \ ; \tag{108}$$

which has necessarily to be less than unity for bound density perturbations.

Accordingly, the sum of initial systematic rotational and peculiar energy, $E'_{rot} + E'_{pec}$, cannot exceed $-E'_{pot} - E'_{osc}$ for bound configurations, i.e. $\mathcal{E}'_{rot} + \mathcal{E}'_{pec} < 1 - \mathcal{E}'_{osc}$. Keeping in mind that Ω_{rec} may safely be put equal to unity and the overdensity index, $\bar{\delta}_{rec}$, amounts to a few percent, it can be seen from Eq. (108) that the sum of parameters, $\mathcal{E}'_{rot} + \mathcal{E}'_{pec}$, cannot

exceed a few percent, or in other words the sum of initial rotational and peculiar energy is two orders of magnitude lower than the initial expansion energy. Then the knowledge of the initial rotational and peculiar velocity field is not essential, and for this reason an initial rigid rotation is assumed, together with a null, initial, peculiar velocity field.

With regard to the final configuration, the simplest case of mass conservation, $M = M'$ or $\beta_M = 1$, and energy conservation, $E = E'$ or $\beta_E = 1$, makes a valid approximation for isolated, overdense regions. On the other hand, merger accretion necessarily implies $\beta_M > 1$ and $\beta_E > 1$. In addition, (complete) virialization, $E_{sel} + 2(E_{rot} + E_{res}) = 0$, may safely be assumed in dealing with density perturbations of galactic size, while it must be released for larger dimensions i.e. clusters of galaxies, where the inner region is relaxed but the outer shells are still infalling.

For representing density profiles of virialized, dark matter haloes, expressed by Eqs. (1), two alternatives will be exploited. One, first proposed by Navarro et al. (1995; 1996; 1997), reads:

$$f(\xi) = \frac{4}{\xi(1+\xi)^2} \ ; \tag{109}$$

and will be quoted in the following as the NFW density profile. One other, first proposed by Moore et al. (1998; 1999), reads:

$$f(\xi) = \frac{2}{\xi^{3/2}(1+\xi^{3/2})} \ ; \tag{110}$$

and will be quoted in the following as the MOA density profile. In both cases, the truncated scaled radius is determined by fitting the results of high-resolution simulations in a CDM cosmological model (Fukushige & Makino 2001) to the selected density profile. For more details, see CM03; Caimmi & Marmo (2004). In addition, both rigid rotation (triaxial configurations) and constant rotational velocity on the equatorial plane (axisymmetric configurations) are assumed. In the latter alternative, both rigid ($\eta_{anm} = 2\eta_{rot} = 1$) and differential (to ensure constant rotational velocity everywhere: $\eta_{anm} = 3\pi/8$, $\eta_{rot} = 3/4$) rotation of the generic, isopycnic surface, are considered. The values of the truncated, scaled radius, and some profile parameters, expressed in Sect. 2 and particularized to both NFW and MOA density profiles, are listed in Tab. 5.

At this stage, the calculations are allowed to start, following the procedure outlined below.

(i) Define the values of the input parameters: the axis ratios, ϵ'_{21} and ϵ'_{31}, the profile parameters, ν'_{sel} and ν'_{ram}, the overdensity index, $\bar{\delta}_{rec}$, the degree of departure from mass conservation, β_M, energy conservation, β_E, angular momentum conservation, β_J, and the virial index, ζ, the last in connection with the final configuration.

(ii) Select a density profile for the final configuration, and calculate the profile parameters, ν_{mas}, ν_{inr}, ν_{sel}.

(iii) Select a velocity profile (of the kind considered in Sect. 2) for the final configuration, and calculate the profile parameters, ν_{anm}, ν_{rot}, ν_{ram}, and the shape parameters, η_{anm}, η_{rot}.

(iv) Select a sequence of homeoidally striated Jacobi ellipsoids (which represent final configurations), where the generalized and effective anisotropy parameters, ζ_p and $\tilde{\zeta}_{pp}$, are kept constant.

(v) Select a value of the axis ratio, ϵ_{21}, of a configuration on the sequence under consideration.

(vi) Calculate the value of the remaining axis ratio, ϵ_{31}.

(vii) Calculate the value of the rotation parameters, h, $\mathcal{E}_{rot}$, υ, λ, and χ_υ, defined by Eqs. (C2), (C3), (C4), (C5), and (C6), respectively.

(viii) Calculate the value of the ratios, $\mathcal{E}'_{rot}/(1-\mathcal{E}'_{osc})$, and a_1/a'_1, defined by Eqs. (77), (79), (80), and (108).

(ix) Select another configuration on the sequence under consideration, and return to (v), unless the whole sequence is covered.

(x) Select another sequence of homeoidally striated Jacobi ellipsoids, where the generalized and effective anisotropy parameters, ζ_{pp} and $\tilde{\zeta}_{pp}$, are kept constant, and return to (v).

(xi) Select another velocity profile for the final configuration, and return to (iv), unless the range of interest is covered.

(xii) Select another density profile for the final configuration, and return to (iii), unless the range of interest is covered.

(xiv) Select another value of the virial index, ζ (in connection with the final configuration), and return to (ii), unless the range of interest is covered.

4.6. Results and discussion

Our attention shall be limited to dark matter haloes hosting giant galaxies, with masses of about $10^{12}\mathrm{m}_\odot$. Accordingly, we assume $\bar{\delta}_{rec} = 0.015$ as a typical overdensity index of the initial configuration, and a virialized final configuration i.e. $\zeta = 1$. In addition, the following range of parameters, $\beta_\mathcal{E}$ and β_a, is considered:

$$\frac{1}{100} \geq \beta_\mathcal{E} \geq \frac{1}{14400} \ ; \qquad 100 \leq \beta_a \leq 14400 \ ; \tag{111}$$

which includes the case $\beta_M = \beta_E = 1$, allowing β_J lie within the range:

$$10 \leq \beta_J \leq 120 \ ; \tag{112}$$

owing to Eq. (81). For sake of simplicity, in what follows the last choice of $(\beta_M, \beta_E, \beta_J)$ will be adopted, but keeping in mind that it is equivalent to any other choice satisfying Eqs. (111), for what will be analysed and discussed.

In particular, three sequences of density profiles with constant anisotropy parameters, $\tilde{\zeta}_{pp}$, are considered, starting from a nonrotating, axisymmetric configuration equal to an oblate ($\epsilon_{31} = 0.5$; $\tilde{\zeta}_{11} = 0.3910$; $\tilde{\zeta}_{33} = 0.2180$), round ($\epsilon_{31} = 1$; $\tilde{\zeta}_{11} = \tilde{\zeta}_{33} = 1/3$), and prolate ($\epsilon_{31} = 2$; $\tilde{\zeta}_{11} = 0.2717$; $\tilde{\zeta}_{33} = 0.4566$) spheroid, respectively.

As in Thuan & Gott (1975) original approach, a limiting configuration exists, which makes the discriminant, expressed by Eq. (78), equal to zero. More flattened configurations are not

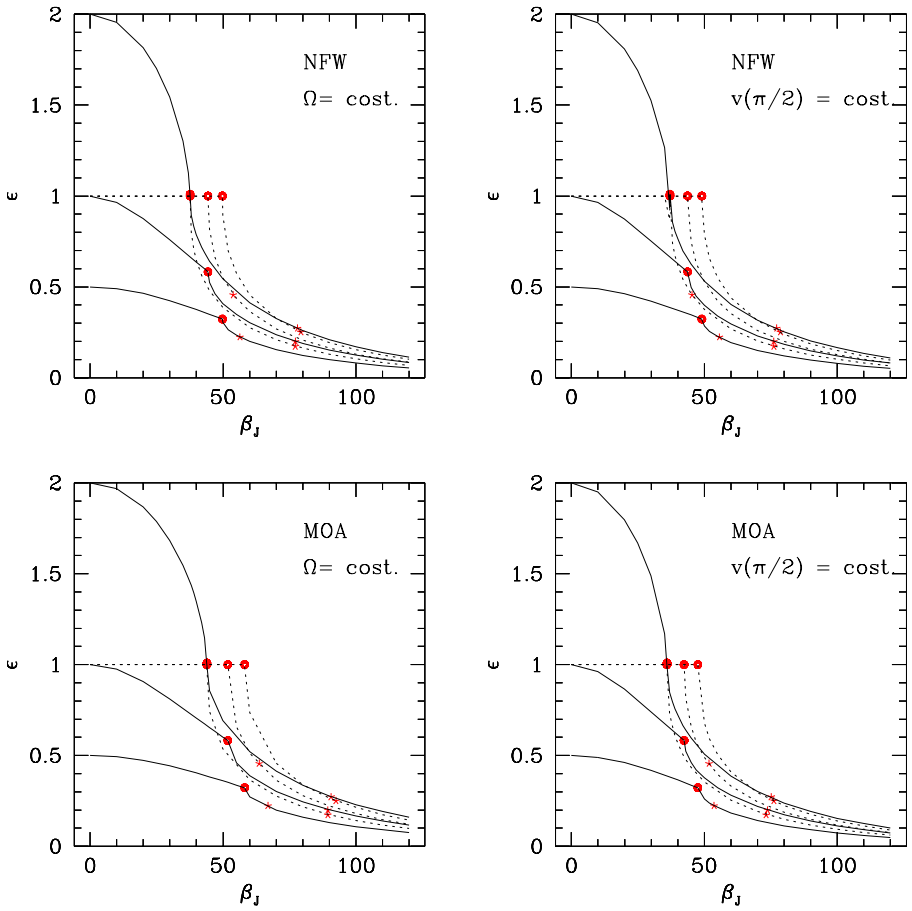

Fig. 5. The axis ratios of the limiting configuration as a function of the parameter, β_J, for sequences of virialized density profiles with constant anisotropy parameters, starting from axisymmetric, nonrotating configurations, defined as: O ($\epsilon_{31} = 0.5$; $\tilde{\zeta}_{11} = 0.3910$; $\tilde{\zeta}_{33} = 0.2180$); S ($\epsilon_{31} = 1$; $\tilde{\zeta}_{11} = \tilde{\zeta}_{33} = 1/3$); P ($\epsilon_{31} = 2$; $\tilde{\zeta}_{11} = 0.2717$; $\tilde{\zeta}_{33} = 0.4566$). The polar and the equatorial axis ratio, ϵ_{31} and ϵ_{21}, are represented by full and dashed curves, respectively. Configurations for which bifurcation from axisymmetric to triaxial density profiles occurs, are marked by filled circles. Pentagon skeletons mark configurations for which the validity of a necessary condition for the occurrence of centrifugal support at the ends of the major axis, is first satisfied. The density profile and the kind of rotation are indicated in each panel. Configurations related to constant rotational velocity on the equatorial plane, $v(\pi/2) = const$, and rigid rotation of isopycnic surfaces, have no physical counterpart for triaxial boundaries.

allowed for the related sequence of density profiles and choice of $(\beta_M, \beta_E, \beta_J)$. The dependence of the axis ratios of the limiting configuration on the parameter, β_J, related to the three sequences mentioned above, is represented in Fig. 5 for NFW and MOA virialized density profiles, characterized by either rigid rotation or constant rotational velocity on the equatorial plane and rigid rotation of isopycnic surfaces. Configurations for which bifurcation from axisymmetric to triaxial density profiles occurs, are marked by filled circles. Pentagon skele-

tons mark configurations for which the validity of a necessary condition for the occurrence of centrifugal support at the ends of the major axis, according to Eq. (65), is first satisfied.

As low values of β_J correspond to bounder final configurations and vice versa, the axis ratio of the limiting configurations are strongly dependent on the sequence under consideration for low values of β_J and vice versa. In other words, a large amount of rotational energy erases the memory of the initial shape, different for different sequences. A complete dissipation of angular momentum, $\beta_J = 0$, yields nonrotating final configurations. In addition, it can be seen from Fig. 5 that a conservation of angular momentum, $\beta_J = 1$, implies final configurations lying near the nonrotating limit.

The density profile and the kind of rotation are indicated in each panel of Fig. 5. Configurations related to constant rotational velocity on the equatorial plane, $v(\pi/2) = const$, and rigid rotation of isopycnic surfaces, have no physical counterpart for triaxial boundaries, but they may be of mathematical interest for comparison with solid-body rotating mass distributions with equal density profile. On the other hand, a change in density profile affects the curves to a smaller extent for configurations with constant rotational velocity on the equatorial plane, with respect to rigidly rotating configurations, as expected.

From this point on, our attention shall be focused on two special values of β_J, namely:

$$\beta_J = 60 \ ; \qquad 0.20 \lesssim (\epsilon_{31})_{lim} \lesssim 0.40 \ ; \qquad 0.30 \lesssim (\epsilon_{21})_{lim} \lesssim 0.50 \ ; \tag{113}$$

$$\beta_J = 120 \ ; \qquad 0.05 \lesssim (\epsilon_{31})_{lim} \lesssim 0.16 \ ; \qquad 0.06 \lesssim (\epsilon_{21})_{lim} \lesssim 0.15 \ ; \tag{114}$$

in connection with NFW density profiles in rigid rotation. An inspection to Fig. 5 shows that the validity of a necessary condition for the occurrence of centrifugal support at the ends of the major axis, according to Eq. (65), may be violated.

The axis ratios of the final configuration, ϵ_{31} and ϵ_{21} (upper panels) and the axis ratio of final to initial configuration, a_1/a'_1 (lower panels), as a function of the parameter, $\chi_{\mathcal{E}} = \mathcal{E}'_{rot}/(1 - \mathcal{E}'_{osc})$, are plotted in Fig. 6 for three sequences of density profiles, O, S, and P, considered earlier, and $\beta_J = 60$ (left panels) and $\beta_J = 120$ (right panels). Each curve on the upper panels is symmetric with respect to a vertical axis, $\chi_{\mathcal{E}} = 0.5$, and is characterized by three extremal points, two maxima and one minimum. The maxima are related to the starting configuration of the sequence, with finite and infinite axes, respectively. On the other hand, the minimum corresponds to the limiting configuration, which exhibits the lowest values of the axis ratios, allowed for the sequence under consideration. Flat configurations occur only in the limit $\beta_J \to +\infty$ unless centrifugal support takes place at the ends of the major axis, from which two flows of dark matter freely stream (see e.g., Jeans 1929, Chap. XIII, § 301, with regard to gaseous nebulae). In addition, larger values of β_J make different curves closer each to the other, and vice versa. The limit, $\chi_{\mathcal{E}} \to 1$, corresponds to unbound configurations $(E = 0)$ which extend to infinite.

The rotation parameters, $\mathcal{E}_{rot}$, h, λ, and υ, (from top left in clockwise sense), and χ_v, related to the final configuration, as a function of the axis ratios, ϵ_{31} and ϵ_{21}, are plotted in

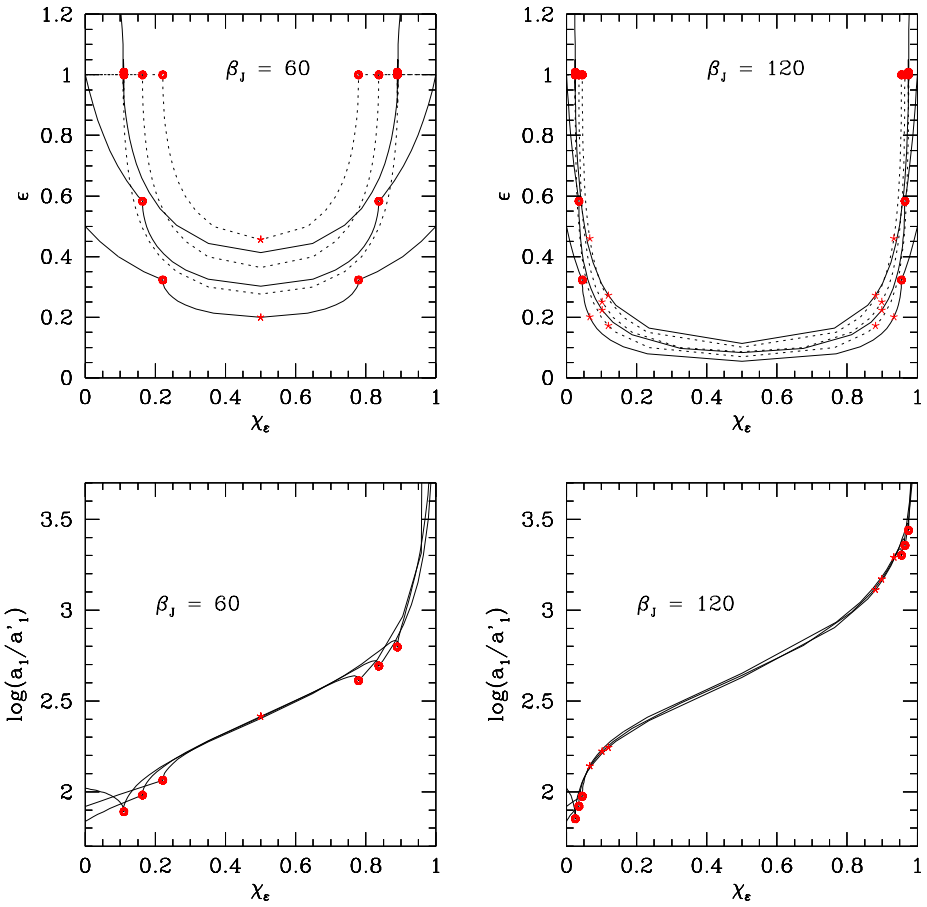

Fig. 6. The axis ratios of the final configuration, ϵ_{31} and ϵ_{21} (upper panels) and the decimal logarithm of the axis ratio, a_1/a_1', of final to initial configuration (lower panels), as a function of the parameter, $\chi_{\mathcal{E}} = \mathcal{E}'_{rot}/(1-\mathcal{E}'_{osc})$, for sequences of virialized density profiles, O, S, and P, considered in Fig. 5, top left panel, related to $\beta_J = 60$ (left panels) and $\beta_J = 120$ (right panels). The curves on the upper panels are symmetric with respect to a vertical axis, $\chi_{\mathcal{E}} = 0.5$. The point of minimum of each curve of the upper panels corresponds to the related, limiting value of the axis ratio, i.e. the lower value allowed along the sequence under consideration. Other captions as in Fig. 5. The limit, $\chi_{\mathcal{E}} \to 1$, is related to unbound configurations $(E = 0)$ which extend to infinite.

Figs. 7 and 8, respectively, for three sequences of density profiles, O, S, and P, considered earlier. The curves are independent of the parameter, β_J, but the limiting values of the axis ratios, related to the selected value of β_J, cannot be exceeded moving from the right to the left along each curve. The horizontal lines correspond to a mean value, $\lambda = 0.0421$, and related variations within one rms error, $\lambda^+ = 0.133$ and $\lambda^- = 0.0133$, consistent with the results of high-resolution numerical simulations (e.g., Bullock et al. 2001; Vitvitska et al. 2002).

Leaving aside peculiar situations such as the occurrence of a major merger near the end of evolution, the main results of high-resolution simulations (e.g., Fukushige & Makino 2001;

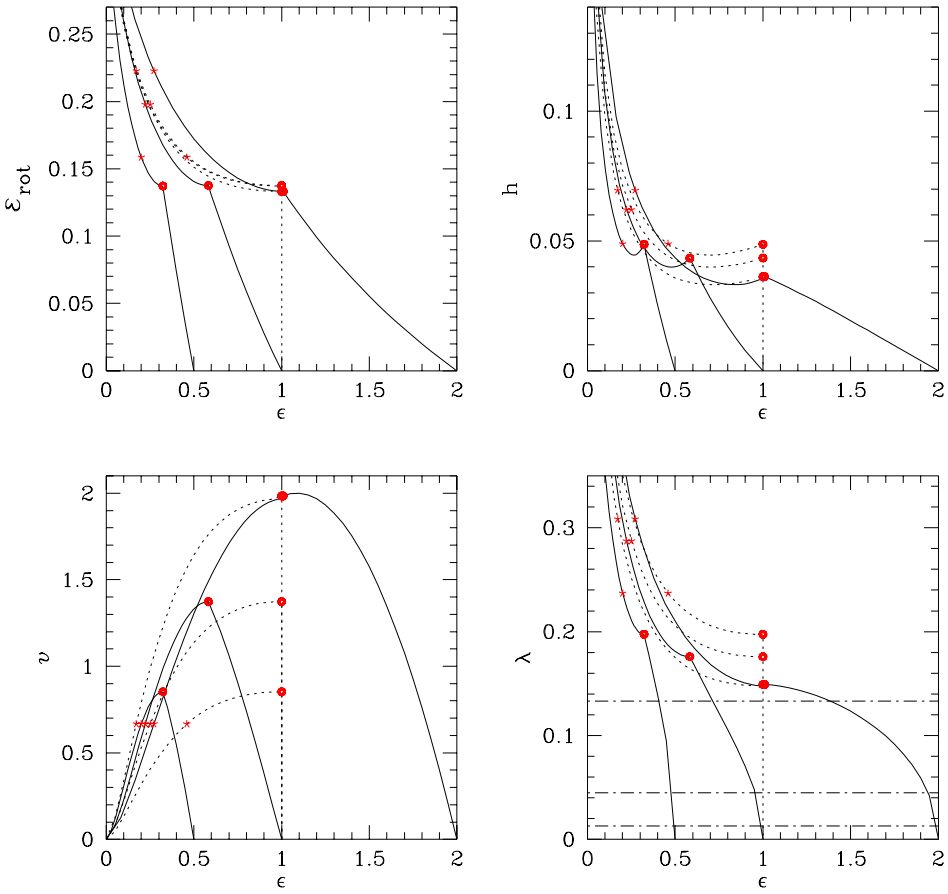

Fig. 7. The rotation parameters, $\mathcal{E}_{rot}$, h, λ, and υ, (from top left in clockwise sense), related to the final configuration, as a function of the axis ratios, ϵ_{31} (full curves) and ϵ_{21} (dashed curves), for sequences of density profiles, O, S, and P, considered in Fig. 5, top left panel. The curves are independent of the parameter, β_J, but the limiting values of the axis ratios, related to β_J, cannot be exceeded moving from the right to the left along each curve. The horizontal lines correspond to a mean value, $\lambda = 0.0421$, and related variations within one rms error, $\lambda^+ = 0.133$ and $\lambda^- = 0.0133$, consistent with results from high-resolution numerical simulations. Other captions as in Fig. 5.

Klypin et al. 2001; Bullock et al. 2001; Vitvitska et al. 2002) may be summarized as follows, to a good extent: (i) a substantial fraction of the initial density perturbation gets virialized; (ii) the density profile may be considered as self-similar and universal; and (iii) the distribution of the rotation parameter, λ, is lognormal with mean value, $0.03 \lesssim \lambda \lesssim 0.05$, and rms error, $0.5 \lesssim \sigma_{\log \lambda} \lesssim 0.7$, in particular $\lambda = 0.0421$, $\sigma_{\log \lambda} = 0.500$.

Accordingly, simulated density profiles with assigned mass, boundary, and rotation parameter, may be compared with their counterparts deduced from the current model. In particular, an inspection of Figs. 6 and 7 shows that, in the range $0.013 \leq \lambda \leq 0.133$, dark matter haloes are close to the starting point of the selected sequence i.e. the nonrotating configuration. Then

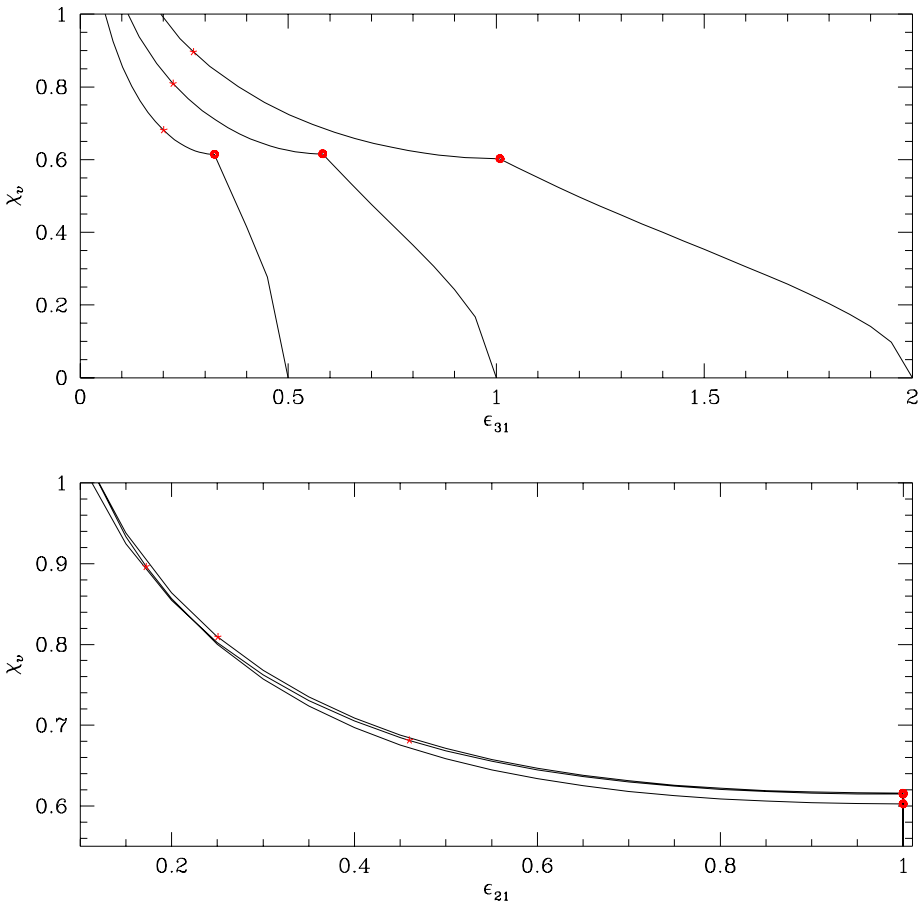

Fig. 8. The rotation parameter, χ_v, related to the final configuration, as a function of the axis ratios, ϵ_{31} (upper panel) and ϵ_{21} (lower panel), for sequences of density profiles, O, S, and P, considered in Fig. 5, top left panel. The curves are independent of the parameter, β_J, but the limiting values of the axis ratios, related to β_J, cannot be exceeded moving from the right to the left along each curve. Other captions as in Fig. 5.

the shape of dark matter haloes is decided mainly by the amount of anisotropy in residual velocity distribution, while the contribution of rotation has only a minor effect on the meridional plane, and no effect on the equatorial plane. This is why bifurcation points occur for larger values of λ. In other words, dark matter haloes may exhibit any shape, provided it is owing mainly to anisotropy in residual velocity distribution and only weakly to systematic rotation.

The analysis of elongated configurations which rotate around the major axis goes beyond a purely academic interest. Empirical evidence in favour of the existence of galaxies with prolate stellar structure, cut equatorially by a gaseous lane, was found long time ago (Bertola & Galletta 1978). The hosting dark haloes could also be prolate and spinning around the symmetry axis. A recent investigation on polar ring galaxies has indicated that the hosting dark haloes are most likely elongated towards the polar ring plane (Iodice et al. 2003), where the rotation axis of the inner body lies.

5. Conclusion

The formulation of the tensor virial equations has been generalized to unrelaxed configurations, where virial equilibrium does not coincide with dynamical (or hydrostatic) equilibrium. Special classes of homeoidally striated ellipsoids have been shown to exhibit similar properties as Jacobi ellipsoids, and to reduce to Jacobi ellipsoids in the limiting situation of homogeneous matter distribution, rigid rotation, and isotropic residual velocity distribution. Accordingly, the above mentioned density profiles have been defined as homeoidally striated, Jacobi ellipsoids. Further investigation has been devoted to the generation of sequences of virial equilibrium configurations, and sequences with constant rotation and anisotropy parameters have been studied with more detail, including both flattened and elongated triaxial (in particular, both oblate and prolate axisymmetric) configurations, and the determination of the related bifurcation points. The explicit expression of a number of rotation parameters, used in literature, and the ratio of rms rotation to rms residual velocity, have also been calculated.

Thuan & Gott (1975) procedure has been generalized to homeoidally striated, Jacobi ellipsoids, and a few limiting situations have also been analysed. An application has been made to dark matter haloes, and calculations have been performed for masses $M \approx 10^{12}\mathrm{m}_{\odot}$ i.e. haloes hosting giant galaxies. The results have been shown to be qualitatively similar to what was found by Thuan & Gott (1975), in particular concerning the occurrence of limiting axis ratios, below which no configuration is allowed for the sequence under consideration. The dependence of the limiting axis ratios on two parameters, related to the degree of change in mass, total energy, and angular momentum, has been illustrated in connection with NFW and MOA density profiles, rotating with constant either angular or linear (on the equatorial plane) velocity, for three special sequences starting from an oblate $(\epsilon_{31} = 0.5)$, round $(\epsilon_{31} = 1)$, and prolate $(\epsilon_{31} = 2)$, nonrotating configuration, respectively.

The dependence of the axis ratios, ϵ_{31} and ϵ_{21}, on the parameter, $\chi_{\mathcal{E}} = \mathcal{E}'_{rot}/(1 - \mathcal{E}'_{osc})$, has been analysed in connection with rigidly rotating, NFW density profiles, for the three special sequences mentioned above. The same has been done for the rotation parameters. Within the range of the rotation parameter, $\exp_{10}(\log\lambda \mp \sigma_{\log\lambda}) = \exp_{10}(-1.3761 \mp 0.500)$, consistent with results from high-resolution numerical simulations, it has been shown that the shape of dark matter haloes is mainly decided by the amount of anisotropy in residual velocity distribution. On the other hand, the contribution of rotation has exhibited only a minor effect on the meridional plane, and no effect on the equatorial plane, as bifurcation points occur for larger values of λ. To this respect, dark matter haloes have been found to resemble giant elliptical galaxies (e.g., Binney 1976; Binney & Tremaine 1987, Chap. 4, § 3).

References

Bertola, F., Galletta, G. 1978, ApJ 226, L115

Binney, J. 1976, MNRAS 177, 19

Binney, J. 1978, MNRAS 183, 501

Binney, J., & Tremaine, S. 1987, *Galactic Dynamics*, Princeton University Press, Princeton

Brosche, P. 1970, A&A 6, 240

Brosche, P., Caimmi, R., & Secco, L. 1983, A&A 125, 338

Bullock, J.S., Dekel, A., Kolatt, T.S., et al. 2001, ApJ 555, 240

Busarello, G., Filippi, S., & Ruffini, R. 1989, A&A 213, 80

Busarello, G., Filippi, S., & Ruffini, R. 1990, A&A 227, 30

Caimmi, R. 1980, ApSS 71, 415

Caimmi, R. 1983, ApSS 93, 403

Caimmi, R., 1991, ApSS 180, 211

Caimmi, R. 1992, AN 313, 165

Caimmi, R. 1993a, ApJ 419, 615

Caimmi, R. 1993b, ApSS 209, 1

Caimmi, R., 1995. ApJ 441, 533

Caimmi, R. 1996a, Acta Cosmologica XXII, 21

Caimmi, R. 1996b, AN 317, 401

Caimmi, R., & Marmo, C. 2003, NewA 8, 119 (CM03)

Caimmi, R., & Marmo, C. 2004, SAJ 169, 11

Chambat, F. 1994, A&A 292, 76

Chandrasekhar, S. 1961, *Hydrodynamic and Hydromagnetic Stability*, Oxford

Chandrasekhar, S. 1969, *Ellipsoidal Figures of Equilibrium*, Yale University Press, New Haven

Chandrasekhar, S., 1962, ApJ 136, 1048

Chandrasekhar, S., & Leboviz, N.R. 1962, ApJ 136, 1082

Fukushige, F., & Makino, J. 2001, ApJ 557, 533

Gradshteyn, I.S., Ryzhik, I.M., 1965. *Table of Integrals, Series, and Products*, Academic Press, New York

Gunn, J.E. 1987, *The Galaxy*, NATO ASI Ser. C207, D. Reidel Publ. Co., Dordrecht, p. 413 74

Iodice, E., Arnaboldi, M., Bournaud, F., et al. 2003, ApJ 585, 730

James, R.A. 1964. ApJ 140, 552

Jeans, J. 1929, *Astronomy and Cosmogony*, Dover Publications, New York, 1961

Klypin, A., Kravtsov, A.V., Bullock, J.S., & Primack, J.R. 2001, ApJ 554, 903

Lai, D., Rasio, F.A., & Shapiro, S.L. 1993, ApJS 88, 205

Landau, L., Lifchitz, E., 1966. *Mecanique*, Mir, Moscow

Moore, B., Governato, F., Quinn, T., Stadel, J., & Lake, G. 1998, ApJ 499, L5

Moore, B., Quinn, T., Governato, F., Stadel, J., & Lake, G. 1999, MNRAS 310, 1147

Navarro, J.F., Frenk, C.S., & White, S.D.M. 1995, MNRAS 275, 720

Navarro, J.F., Frenk, C.S., & White, S.D.M. 1996, ApJ 462, 563

Navarro, J.F., Frenk, C.S., & White, S.D.M. 1997, ApJ 490, 493

Ostriker, J.P., & Peebles, P.J.E. 1973, ApJ 186, 467

Pacheco, F., Pucacco, G., & Ruffini, R. 1986, A&A 161, 39

Pacheco, F., Pucacco, G., Ruffini, R., & Sebastiani, G. 1989, A&A 210, 42

Peebles, P.J.E. 1969, ApJ 169, 393

Roberts, P.H. 1962, ApJ 136, 1108

Spiegel, M.R., 1968. *Mathematical Handbook of Formulas and Tables*, Schaum's Outline Series, McGraw-Hill, Inc., New York

Tassoul, J.L. 1978, *Theory of Rotating Stars*, Princeton University Press, Princeton

Thuan, T.X., & Gott, J.R., III, 1975, Nature 257, 774

Vandervoort, P.O., 1980, ApJ 240, 478

Vandervoort, P.O., Welty, D.E. 1981, ApJ 248, 504

Vitvitska, M., Klypin, A.A., Kravstov, A.V., et al. 2002, ApJ 581, 799

Wiegandt, R., 1982a, A&A 105, 326

Wiegandt, R., 1982b, A&A 106, 240

Zeldovich, J.B., & Novikov, I.D. 1982, *Struttura ed evoluzione dell'Universo*, Mir, Moscow

Appendix A: Different normalizations for homeoidally striated density profiles

With regard to homeoidally striated density profiles, defined by Eqs. (1), the mass, the inertia tensor, and the self-energy tensor, may be expressed as (CM03):

$$M = \nu^{\dagger}_{mas} M^{\dagger} \ ; \tag{A1}$$

$$I_{pq} = \delta_{pq} \nu^{\dagger}_{inr} M^{\dagger} (a^{\dagger}_{p})^{2} \ ; \tag{A2}$$

$$(E_{sel})_{pq} = -\nu^{\dagger}_{sel} \frac{G(M^{\dagger})^{2}}{a^{\dagger}_{1}} (B_{sel})_{pq} \ ; \tag{A3}$$

where the profile parameters, $\nu^{\dagger}$, take the explicit form (CM03):

$$\nu^{\dagger}_{mas} = \frac{3}{2} \int_{0}^{\Xi} F(\xi) \, \mathrm{d}\xi \ ; \tag{A4}$$

$$\nu^{\dagger}_{inr} = \frac{3}{2} \int_{0}^{\Xi} F(\xi) \xi^{2} \, \mathrm{d}\xi \ ; \tag{A5}$$

$$\nu^{\dagger}_{sel} = \frac{9}{16} \int_{0}^{\Xi} F^{2}(\xi) \, \mathrm{d}\xi \ ; \tag{A6}$$

and the function, $F(\xi)$, has the definition (Roberts 1962):

$$F(\xi) = 2 \int_{\xi}^{\Xi} f(\xi') \xi' \, \mathrm{d}\xi' \ ; \tag{A7}$$

where the function, $f(\xi)$, corresponds to the density profile, according to Eqs. (1). It can easily be seen that the following relations hold:

$$F(\Xi) = 0 \ ; \qquad \frac{\mathrm{d}F}{\mathrm{d}\xi} = -2\xi f(\xi) \ ; \tag{A8}$$

and an integration by parts shows that:

$$\int_{0}^{\Xi} f(\xi) \xi^{n} \, \mathrm{d}\xi = \frac{n-1}{2} \int_{0}^{\Xi} F(\xi) \xi^{n-2} \, \mathrm{d}\xi \ ; \qquad n > 1 \ ; \tag{A9}$$

which allows the calculation of the profile parameters. The scaling mass, $M^{\dagger}$, has the same definition in CM03 as its counterpart, M_0, in the current paper, according to Eq.(6). Then the following relation holds:

$$M^{\dagger} = M_{0} \ ; \tag{A10}$$

for further details, see CM03.

The mass, the inertia tensor, and the self-energy tensor, in the current paper are expressed by Eqs.(2), (3), and (4), respectively. The comparison with their counterparts, expressed by Eqs. (A1), (A2), and (A3), yields:

$$\nu_{mas} = \nu^{\dagger}_{mas} \ ; \tag{A11}$$

$$\nu_{inr} = \nu^{\dagger}_{inr} \frac{M^{\dagger}}{M} \frac{(a^{\dagger}_p)^2}{a_p^2} \ ; \tag{A12}$$

$$\nu_{sel} = \nu^{\dagger}_{sel} \left(\frac{M^{\dagger}}{M} \right)^2 \frac{a_1}{a^{\dagger}_1} \ ; \tag{A13}$$

where the last two relations, owing to Eqs. (1b), (2), (A10), and (A11), may be written under the equivalent form:

$$\nu_{inr} = \frac{\nu^{\dagger}_{inr}}{\nu^{\dagger}_{mas} \Xi^2} \ ; \tag{A14}$$

$$\nu_{sel} = \frac{\nu^{\dagger}_{sel} \Xi}{(\nu^{\dagger}_{mas})^2} \ ; \tag{A15}$$

and the profile parameters, $\nu^{\dagger}_{mas}$, $\nu^{\dagger}_{inr}$, $\nu^{\dagger}_{sel}$, are expressible as functions of the scaled radius, Ξ (CM03).

The angular-momentum vector and the rotational-energy tensor, for the special rotational velocity fields discussed in Sect. 2, may be expressed as (CM03):

$$J_s = \delta_{s3} \eta^{\dagger}_{anm} \nu^{\dagger}_{anm} M^{\dagger} a^{\dagger}_p (1 + \epsilon^2_{qp}) (v^{\dagger}_{rot})_p \ ; \quad p \neq q \neq s \ ; \tag{A16}$$

$$(E_{rot})_{pq} = \delta_{pq} (1 - \delta_{p3}) \eta^{\dagger}_{rot} \nu^{\dagger}_{rot} M^{\dagger} \left[(v^{\dagger}_{rot})_p \right]^2 \ ; \tag{A17}$$

and the related module (angular momentum) and trace (rotational energy), respectively, as:

$$J = \eta^{\dagger}_{anm} \nu^{\dagger}_{anm} M^{\dagger} a^{\dagger}_1 (1 + \epsilon^2_{21}) (v^{\dagger}_{rot})_1 \ ; \tag{A18}$$

$$E_{rot} = \eta^{\dagger}_{rot} \nu^{\dagger}_{rot} M^{\dagger} (1 + \epsilon^2_{21}) \left[(v^{\dagger}_{rot})_1 \right]^2 \ ; \tag{A19}$$

where $(v^{\dagger}_{rot})_p$ is the rotational velocity at the top axis, $a^{\dagger}_p$, of the reference isopycnic surface.

The profile parameters, $\nu^{\dagger}$, and the shape parameters, $\eta^{\dagger}$, take the explicit form (CM03):

$$\nu^{\dagger}_{anm} = \int_0^{\Xi} \frac{\Omega(\xi, 0)}{\Omega(1, 0)} f(\xi) \xi^4 \, \mathrm{d}\xi \ ; \tag{A20}$$

$$\nu^{\dagger}_{rot} = \int_0^{\Xi} \frac{\Omega^2(\xi, 0)}{\Omega^2(1, 0)} f(\xi) \xi^4 \, \mathrm{d}\xi \ ; \tag{A21}$$

$$\eta^{\dagger}_{anm} = \frac{3}{4} \epsilon^4 \int_{-\pi/2}^{+\pi/2} \frac{\Omega(1, \theta)}{\Omega(1, 0)} \frac{\sin^3 \theta \, \mathrm{d}\theta}{(\cos^2 \theta + \epsilon^2 \sin^2 \theta)^{5/2}} \ ; \tag{A22}$$

$$\eta^{\dagger}_{rot} = \frac{3}{8} \epsilon^4 \int_{-\pi/2}^{+\pi/2} \frac{\Omega^2(1, \theta)}{\Omega^2(1, 0)} \frac{\sin^3 \theta \, \mathrm{d}\theta}{(\cos^2 \theta + \epsilon^2 \sin^2 \theta)^{5/2}} \ ; \tag{A23}$$

where ϵ is the ratio of polar to equatorial axis and θ is the azimuthal angle. It is worth of note that the above expressions for the shape parameters, $\eta^{\dagger}$, hold for axisymmetric configurations. The shape parameters, η, are also expressed by Eqs. (A22) and (A23), provided $\Omega(1, \theta)$ and $\Omega(1, 0)$ therein are replaced by $\Omega(\Xi, \theta)$ and $\Omega(\Xi, 0)$, respectively. The extension of the above definitions and results to (necessarily) solid-body rotating, triaxial configurations, yields $\eta_{anm} = 1$, $\eta_{rot} = 1/2$, according to Eqs. (7)-(10). For further details, see CM03.

The angular-momentum vector, the rotational-energy tensor, the angular momentum, and the rotational energy, in the current paper are expressed by Eqs. (18), (19), and (20), (21),

respectively. The comparison with their counterparts, Eqs. (A16), (A17), and (A18), (A19), respectively, yields:

$$\nu_{anm} = \nu^{\dagger}_{anm} \frac{\eta^{\dagger}_{anm}}{\eta_{anm}} \frac{M^{\dagger}}{M} \frac{a^{\dagger}_p}{a_p} \frac{(v^{\dagger}_{rot})_p}{(v_{rot})_p} \ ; \qquad p = 1, 2 \ ; \tag{A24}$$

$$\nu_{rot} = \nu^{\dagger}_{rot} \frac{\eta^{\dagger}_{rot}}{\eta_{rot}} \frac{M^{\dagger}}{M} \frac{(v^{\dagger}_{rot})^2_p}{(v_{rot})^2_p} \ ; \qquad p = 1, 2 \ ; \tag{A25}$$

where, owing to Eq. (12), $\eta_{anm} = \eta^{\dagger}_{anm}$ and $\eta_{rot} = \eta^{\dagger}_{rot}$. Then Eqs. (A24) and (A25), by use of (1b), (2), and (A10), take the equivalent form:

$$\nu_{anm} = \frac{\nu^{\dagger}_{anm}}{\nu^{\dagger}_{mas} \Xi} \frac{(v^{\dagger}_{rot})_p}{(v_{rot})_p} = \frac{\nu^{\dagger}_{anm}}{\nu^{\dagger}_{mas} \Xi^2} \frac{\Omega(1,0)}{\Omega(\Xi,0)} \ ; \qquad p = 1, 2 \ ; \tag{A26}$$

$$\nu_{rot} = \frac{\nu^{\dagger}_{rot}}{\nu^{\dagger}_{mas}} \frac{(v^{\dagger}_{rot})^2_p}{(v_{rot})^2_p} = \frac{\nu^{\dagger}_{rot}}{\nu^{\dagger}_{mas} \Xi^2} \frac{\Omega^2(1,0)}{\Omega^2(\Xi,0)} \ ; \qquad p = 1, 2 \ ; \tag{A27}$$

where $(v^{\dagger}_{rot})_p/(v_{rot})_p = 1/\Xi$ if the system is in rigid rotation, and $(v^{\dagger}_{rot})_p/(v_{rot})_p = 1$ if the rotational velocity is constant on the equatorial plane. The profile parameters, $\nu^{\dagger}_{anm}$, $\nu^{\dagger}_{rot}$, are expressible as functions of the scaled radius, Ξ (CM03).

The above results allow the calculation of the profile parameters, ν, appearing in the text. The corresponding, explicit expressions, may be seen in Caimmi & Marmo (2004).

Appendix B: Limiting configurations

The general expressions of the shape factors, A_p, and related quantities, for limiting configurations of ellipsoidal shape reduce to undetermined expressions of the kind $0/0$, ∞/∞, *et similia* (e.g., Caimmi 1991, 1992, 1995). Then explicit calculations are needed for round, oblate, prolate, flat, and oblong configurations, which can be found in the above quoted references. Though flat and oblong configurations are dynamically unstable (e.g., Jeans 1929, Chap. IX), they shall also be included for sake of completeness. Accordingly, the expression of the shape factors in the self-energy tensor, $(B_{sel})_{pp} = \epsilon_{p2}\epsilon_{p3}A_p$, see Eq. (5), must be determined even for flat and oblong configurations.

The shape factors, A_p, depend on the axis ratios, via elliptic integrals of first and second kind (e.g., Caimmi 1992):

$$F(\beta, p) = \int_0^{\beta} \frac{\mathrm{d}\phi}{\sqrt{1 - p^2 \sin^2 \phi}} \ ; \qquad E(\beta, p) = \int_0^{\beta} \sqrt{1 - p^2 \sin^2 \phi} \, \mathrm{d}\phi \ ; \tag{B1a}$$

$$\beta = \arccos \epsilon_{31} \ ; \qquad p = \frac{e_{21}}{e_{31}} \ ; \qquad e_{pq} = \sqrt{1 - \epsilon^2_{pq}} \ ; \tag{B1b}$$

where $\beta = \pi/2$ for both flat and oblong configurations, while $p = e_{21}$ and $p = 1$ for flat and oblong configurations, respectively.

With regard to the self-energy tensor, by use of the general expression of the shape factors, A_p, derived in Caimmi (1992; therein defined as $\hat{\alpha}_p$), the flat limit ($\epsilon_{21} > 0$, $\epsilon_{31} \to 0$) reads:

$$(B_{sel})_{11} = \epsilon_{12}\epsilon_{13}A_1 = \frac{2}{e^2_{21}} \left[F\left(\frac{\pi}{2}, e_{21}\right) - E\left(\frac{\pi}{2}, e_{21}\right) \right] = b_1 \ ; \tag{B2a}$$

$$(B_{sel})_{22} = \epsilon_{22}\epsilon_{23}A_2 = \frac{2}{e^2_{21}} \left[E\left(\frac{\pi}{2}, e_{21}\right) - \epsilon^2_{21} F\left(\frac{\pi}{2}, e_{21}\right) \right] = b_2 \ ; \tag{B2b}$$

$$(B_{sel})_{33} = \epsilon_{32}\epsilon_{33}A_3 = \frac{2}{e^2_{21}} \left[-e^2_{21} E\left(\frac{\pi}{2}, e_{21}\right) + \frac{\epsilon_{31}}{\epsilon_{21}} e_{21} \right] = 0 \ ; \tag{B2c}$$

and the special case of the oblate, flat limit ($\epsilon_{21} = 1$, $\epsilon_{31} \to 0$) reads:

$$(B_{sel})_{11} = (B_{sel})_{22} = \lim_{\epsilon_o \to 0} \left(\epsilon_o^{-1} \alpha\right) = \frac{\pi}{2} \ ; \qquad (B_{sel})_{33} = \lim_{\epsilon_o \to 0} (\epsilon_o \gamma) = 0 \ ; \tag{B3a}$$

$$\epsilon_o = \epsilon_{31} = \epsilon_{32} \ ; \qquad \alpha = \lim_{\epsilon_{21} \to 1} A_1 = \lim_{\epsilon_{21} \to 1} A_2 \ ; \qquad \gamma = \lim_{\epsilon_{21} \to 1} A_3 \ ; \tag{B3b}$$

for further details see e.g., Caimmi (1991).

Oblong configurations may be conceived in a twofold manner, according if $\epsilon_{21} \to \epsilon_{31} = 0$ (flat-oblong, hereafter quoted as f-oblong) or $\epsilon_{21} = \epsilon_{31} \to 0$ (prolate-oblong, hereafter quoted as p-oblong). In any case, $\beta \to \pi/2$, $p \to 1$, $e_{21} \to 1$, and Eqs. (B1a) reduce to:

$$\lim_{\epsilon_{21} \to 0} F\left(\frac{\pi}{2}, e_{21}\right) = \lim_{x \to \pi/4} \ln \frac{1 + \tan x}{1 - \tan x} = +\infty \ ; \qquad E\left(\frac{\pi}{2}, 1\right) = 1 \ ; \tag{B4}$$

in addition, using the series development of the complete elliptic integral of first kind and Wallis' product (e.g., Spiegel 1968, §§ 34.2 and 38.9) yields:

$$\lim_{\epsilon_{21} \to 0} \epsilon_{21}^2 F\left(\frac{\pi}{2}, e_{21}\right) = \frac{\pi}{2} \lim_{n \to +\infty} \left[\frac{1 \cdot 3 \cdot \ldots \cdot (2n-1)}{2 \cdot 4 \cdot \ldots \cdot 2n}\right]^2 = \lim_{n \to +\infty} \frac{1}{2n+1} = 0 \ ; \tag{B5}$$

with regard to f-oblong configurations, Eqs. (B2) reduce to:

$$(B_{sel})_{11} = +\infty \ ; \qquad (B_{sel})_{22} = 2 \ ; \qquad (B_{sel})_{33} = 0 \ ; \tag{B6}$$

on the other hand, with regard to p-oblong configurations, the shape factors in the self-energy tensor take the expression:

$$(B_{sel})_{11} = \lim_{\epsilon_p \to 0} \left(\epsilon_p^{-2} \gamma\right) = \lim_{\epsilon \to +\infty} \epsilon^2 \frac{2}{\epsilon^2 - 1} \left[\epsilon \frac{\operatorname{arcsinh} \sqrt{\epsilon^2 - 1}}{\sqrt{\epsilon^2 - 1}} - 1\right] = +\infty \ ; \tag{B7a}$$

$$(B_{sel})_{22} = (B_{sel})_{33} = \lim_{\epsilon_p \to 0} \alpha = \lim_{\epsilon \to +\infty} \frac{\epsilon}{\epsilon^2 - 1} \left[\epsilon - \frac{\operatorname{arcsinh} \sqrt{\epsilon^2 - 1}}{\sqrt{\epsilon^2 - 1}}\right] = 1 \ ; \tag{B7b}$$

$$\epsilon_p = \epsilon^{-1} = \epsilon_{31} = \epsilon_{21} \ ; \qquad \alpha = \lim_{\epsilon_{21} \to \epsilon_{31}} A_1 \ ; \qquad \gamma = \lim_{\epsilon_{21} \to \epsilon_{31}} A_2 = \lim_{\epsilon_{21} \to \epsilon_{31}} A_3 \ ; \tag{B7c}$$

for further details see Caimmi (1991).

The comparison between Eqs. (B6) and (B7) discloses that the shape factors in the self-energy tensor exhibit a discontinuity passing from f-oblong to p-oblong configurations (e.g., Caimmi 1993b). The values of the axis ratios, ϵ_{21} and ϵ_{31}, the shape factors, A_p and $(B_{sel})_{pp}$, related to limiting configurations of ellipsoidal shape, are listed in Tab. B1 where the upper part, containing the shape factors, A_p, has been taken from Caimmi (1995). The range of validity of the independent variables, ϵ_f, ϵ_p, ϵ_o, and ϵ, and the definition of the functions, α, γ, are:

$$0 < \epsilon_f \leq 1 \ ; \qquad 0 < \epsilon_p < 1 \ ; \qquad 0 < \epsilon_o < 1 \ ; \tag{B8a}$$

$$0 < \epsilon < 1 \ , \ \text{oblate}; \qquad 1 < \epsilon < +\infty \ , \ \text{prolate}; \tag{B8b}$$

$$\alpha = \begin{cases} \dfrac{\epsilon}{1 - \epsilon^2} \left[\dfrac{\arcsin(1 - \epsilon^2)^{1/2}}{(1 - \epsilon^2)^{1/2}} - \epsilon\right] \ ; & \text{oblate;} \\ \dfrac{\epsilon}{\epsilon^2 - 1} \left[\epsilon - \dfrac{\operatorname{arcsinh}(\epsilon^2 - 1)^{1/2}}{(\epsilon^2 - 1)^{1/2}}\right] \ ; & \text{prolate;} \end{cases} \tag{B9a}$$

$$\gamma = \begin{cases} \dfrac{2}{1-\epsilon^2}\left[1-\epsilon\dfrac{\arcsin(1-\epsilon^2)^{1/2}}{(1-\epsilon^2)^{1/2}}\right] \ ; & \text{oblate;} \\ \dfrac{2}{\epsilon^2-1}\left[\epsilon\dfrac{\operatorname{arcsinh}(\epsilon^2-1)^{1/2}}{(\epsilon^2-1)^{1/2}}-1\right] \ ; & \text{prolate;} \end{cases} \tag{B9b}$$

and the functions, b_1 and b_2, are expressed by Eqs. (B2a) and (B2b). For further details, see Caimmi (1995).

Appendix C: Expression of anisotropy and rotation parameters in compact notation

The effective anisotropy parameters, $\tilde{\zeta}_{pp}$, expressed by Eqs. (47), and the rotation parameters, h, $\mathcal{E}_{rot}$, υ, λ, and χ_υ, expressed by Eqs. (44), (45), (46), (54), and (57), respectively, may be written in compact notation, using Eqs. (67) and (68). The result is:

$$\tilde{\zeta}_{pp} = \frac{\zeta_{pp}}{\zeta} = \frac{\mathcal{S}_{pp}}{\mathcal{S}}\left[1-2h\frac{\mathcal{R}_{pp}}{\mathcal{S}_{pp}}\right]\left[1-2h\frac{\mathcal{R}}{\mathcal{S}}\right]^{-1} \ ; \qquad p=1,2,3 \ ; \tag{C1}$$

with regard to anisotropy parameters;

$$h = \frac{1}{2}\frac{\mathcal{S}}{\mathcal{R}}\left[1-\frac{\zeta}{\zeta_{33}}\frac{\mathcal{S}_{33}}{\mathcal{S}}\right] \ ; \tag{C2}$$

$$\mathcal{E}_{rot} = \frac{\mathcal{R}}{\mathcal{S}}h \ ; \tag{C3}$$

$$\upsilon = \frac{1}{3}\frac{1}{\eta_{rot}\nu_{rot}}\frac{\epsilon_{21}\epsilon_{31}}{1+\epsilon_{21}^2}\mathcal{S}\left[1-\frac{\zeta}{\zeta_{33}}\frac{\mathcal{S}_{33}}{\mathcal{S}}\right] \ ; \tag{C4}$$

$$\lambda^2 = \frac{1}{4}\frac{\mathcal{S}^2}{\mathcal{R}}\left[1-\frac{\zeta}{\zeta_{33}}\frac{\mathcal{S}_{33}}{\mathcal{S}}\right]\left[1-\frac{1-\zeta}{\zeta}\frac{\zeta}{\zeta_{33}}\frac{\mathcal{S}_{33}}{\mathcal{S}}\right] \ ; \tag{C5}$$

$$\chi_\upsilon^2 = \zeta\left[\frac{\zeta_{33}}{\zeta}\frac{\mathcal{S}}{\mathcal{S}_{33}}-1\right] \ ; \tag{C6}$$

with regard to rotation parameters.

Finally, the combination of Eqs. (C2), (C4), (C5), and (C6) yields:

$$\upsilon = \frac{2}{3}\frac{1}{\eta_{rot}\nu_{rot}}\frac{\epsilon_{21}\epsilon_{31}}{1+\epsilon_{21}^2}\mathcal{R}h \ ; \tag{C7}$$

$$\lambda^2 = \frac{1}{2}\mathcal{S}h\left[1-\frac{1-\zeta}{\zeta}\frac{\zeta}{\zeta_{33}}\frac{\mathcal{S}_{33}}{\mathcal{S}}\right] \ ; \tag{C8}$$

$$\chi_\upsilon^2 = \zeta\frac{2\mathcal{R}h}{\mathcal{S}-2\mathcal{R}h} \ ; \tag{C9}$$

which allows a connection between different rotation parameters.

An inspection of Eq. (C1) shows that the rotation parameter, h, attains the special values:

$$h = \frac{1}{2}\frac{\mathcal{S}_{qq}}{\mathcal{R}_{qq}} \ ; \qquad \tilde{\zeta}_{qq} = 0 \ ; \qquad q=1,2 \ ; \tag{C10a}$$

$$h = \frac{1}{2}\frac{\mathcal{S}-\mathcal{S}_{pp}}{\mathcal{R}-\mathcal{R}_{pp}} \ ; \qquad \tilde{\zeta}_{pp} = 1 \ ; \qquad p=1,2,3 \ ; \tag{C10b}$$

$$h = 0 \ ; \qquad \tilde{\zeta}_{pp} = \frac{\mathcal{S}_{pp}}{\mathcal{S}} \ ; \qquad p=1,2,3 \ ; \tag{C10c}$$

where the last relation is equivalent to Eq. (48).

ϵ_{31}	ϵ_{21}	$\mathcal{E}_{rot}$	h_N	υ_N	λ_N	χ_N
1.000000	1.00	0.0000000	0.0000000	0.00000000	0.000000	0.000000
0.950000	1.00	0.0136423	0.0554973	0.00878707	0.237573	0.167481
0.900000	1.00	0.0279335	0.115614	0.0173421	0.345874	0.243255
0.850000	1.00	0.0429239	0.180831	0.0256177	0.436408	0.306447
0.800000	1.00	0.0586689	0.251690	0.0335587	0.519556	0.364604
0.750000	1.00	0.0752304	0.328809	0.0411011	0.599400	0.420843
0.700000	1.00	0.0926773	0.412889	0.0481704	0.678136	0.476999
0.650000	1.00	0.111086	0.504734	0.0546795	0.757185	0.534446
0.600000	1.00	0.130544	0.605265	0.0605265	0.837600	0.594425
0.582724	**1.00**	**0.137528**	**0.642207**	**0.0623716**	**0.865863**	**0.615969**
0.567738	0.95	0.137631	0.627187	0.0623058	0.866686	0.616287
0.551873	0.90	0.137962	0.614355	0.0620944	0.869331	0.617310
0.535058	0.85	0.138559	0.603917	0.0617145	0.874109	0.619154
0.517216	0.80	0.139466	0.596127	0.0611395	0.881390	0.621957
0.498264	0.75	0.140736	0.591305	0.0603394	0.891630	0.625885
0.478110	0.70	0.142431	0.589855	0.0592799	0.905387	0.631136
0.456652	0.65	0.144629	0.592298	0.0579219	0.923359	0.637951
0.433781	0.60	0.147422	0.599309	0.0562217	0.946423	0.646627
0.409377	0.55	0.150922	0.611785	0.0541300	0.975705	0.657530
0.383309	0.50	0.155270	0.630931	0.0515928	1.01267	0.671126
0.355436	0.45	0.160640	0.658405	0.0485518	1.05927	0.688014
0.325609	0.40	0.167257	0.696539	0.0449463	1.11817	0.708986
0.293667	0.35	0.175409	0.748717	0.0407171	1.19312	0.735119
0.259447	0.30	0.185482	0.820038	0.0358145	1.28960	0.767941
0.222783	0.25	0.198006	0.918565	0.0302122	1.41609	0.809731
0.183524	0.20	0.213754	0.105795	0.0239349	1.58664	0.864147
0.141550	0.15	0.233939	0.126381	0.0171106	1.82719	0.937692
0.968152	0.10	0.260769	0.159292	0.0100787	2.19478	1.04405
0.494435	0.05	0.299688	0.222228	0.00364434	2.86687	1.22315
0.000000	0.00	0.500000	$+\infty$	0.00000000	$+\infty$	$+\infty$

Table 2. Values of axis ratios, ϵ_{31} and ϵ_{21}, and normalized rotation parameters, $\mathcal{E}_{rot}$, h_N, υ_N, λ_N, χ_N, related to a sequence of virial equilibrium configurations with anisotropy parameters, $\tilde{\zeta}_{11} = \tilde{\zeta}_{22} = \tilde{\zeta}_{33} = 1/3$. The polar axis ratio of the initial nonrotating configuration is $\epsilon_{31} = 1$. Values at the bifurcation point are listed on the boldface line.

ϵ_{31}	ϵ_{21}	$\mathcal{E}_{rot}$	h_N	υ_N	λ_N	χ_N
2.00000	1.00	0.00000000	0.0000000	0.00000000	0.000000	0.0000000
1.95000	1.00	0.00478379	0.0286995	0.00932733	0.207471	0.0982853
1.90000	1.00	0.00971323	0.0574460	0.0181912	0.291439	0.140753
1.85000	1.00	0.0147955	0.0862190	0.0265842	0.354412	0.174624
1.80000	1.00	0.0200384	0.114995	0.0344986	0.406180	0.204328
1.75000	1.00	0.0254502	0.143749	0.0419268	0.450536	0.231582
1.70000	1.00	0.0310397	0.172451	0.0488610	0.489413	0.257271
1.65000	1.00	0.0368164	0.201067	0.0552935	0.523951	0.281932
1.60000	1.00	0.0427906	0.229562	0.0612164	0.554875	0.305926
1.55000	1.00	0.0489731	0.257892	0.0666221	0.582678	0.329517
1.50000	1.00	0.0553759	0.286012	0.0715029	0.607705	0.352910
1.45000	1.00	0.0620118	0.313867	0.0758512	0.630201	0.376275
1.40000	1.00	0.0688944	0.341399	0.0796598	0.650340	0.399761
1.35000	1.00	0.0760387	0.368540	0.0829216	0.668248	0.423501
1.30000	1.00	0.0834610	0.395215	0.0856298	0.684008	0.447625
1.25000	1.00	0.0911788	0.421336	0.0877783	0.697672	0.472259
1.20000	1.00	0.0992113	0.446806	0.0893613	0.709265	0.497534
1.15000	1.00	0.107579	0.471516	0.0903739	0.718791	0.523586
1.10000	1.00	0.116305	0.495340	0.0908123	0.726229	0.550563
1.05000	1.00	0.125415	0.518135	0.0906737	0.731541	0.578628
1.00884	**1.00**	**0.133221**	**0.536015**	**0.0901254**	**0.734279**	**0.602676**
0.982862	0.95	0.133325	0.518938	0.0892464	0.728588	0.602997
0.955297	0.90	0.133660	0.508463	0.0889593	0.730978	0.604029
0.926018	0.85	0.134263	0.500075	0.0884430	0.735296	0.605890
0.894889	0.80	0.135180	0.494001	0.0876613	0.741881	0.608720
0.861761	0.75	0.136465	0.490528	0.0865726	0.751151	0.612687
0.826476	0.70	0.138183	0.490021	0.0851292	0.763622	0.617993
0.788860	0.65	0.140412	0.492953	0.0832766	0.779942	0.624884
0.748729	0.60	0.143247	0.499946	0.0809524	0.800933	0.633663
0.705885	0.55	0.146806	0.511829	0.0780864	0.827656	0.644711
0.660119	0.50	0.151235	0.529730	0.0745994	0.861506	0.658506
0.611212	0.45	0.156719	0.555209	0.0704044	0.904353	0.675673
0.558939	0.40	0.163494	0.590488	0.0654076	0.958773	0.697036
0.503073	0.35	0.171870	0.638821	0.0595133	1.02842	0.723729
0.443394	0.30	0.182258	0.705156	0.0526322	1.11870	0.757365
0.379704	0.25	0.195231	0.797402	0.0447006	1.23801	0.800368
0.311845	0.20	0.211623	0.929083	0.0357161	1.40036	0.856647
0.239733	0.15	0.232741	1.12576	0.0258135	1.63179	0.933190
0.163419	0.10	0.260936	1.44447	0.0154269	1.98960	1.04474
0.0832065	0.05	0.301873	2.06324	0.00569398	2.65204	1.23435
0.0000000	0.00	0.500000	$+\infty$	0.00000000	$+\infty$	$+\infty$

Table 3. Values of axis ratios, ϵ_{31} and ϵ_{21}, and normalized rotation parameters, $\mathcal{E}_{rot}$, h_N, υ_N, λ_N, χ_N, related to a sequence of virial equilibrium configurations with anisotropy parame-

$\tilde{\zeta}_{33}$	$(\epsilon_{31})_i$	$(\epsilon_{31})_b$	$(\mathcal{E}_{rot})_b$	$(h_N)_b$	$(\upsilon_N)_b$	$(\lambda_N)_b$	$(\chi_N)_b$
0.0582397	0.10000	0.722934	0.129818	0.780139	0.00939982	1.08262	0.592188
0.107390	0.20000	0.139949	0.132948	0.768228	0.0179188	1.05346	0.601834
0.149487	0.30000	0.203842	0.134996	0.753170	0.0255879	1.02495	0.608151
0.185995	0.40000	0.264590	0.136320	0.736767	0.0324902	0.997747	0.612238
0.217996	0.50000	0.322650	0.137144	0.719984	0.0387171	0.972086	0.614782
0.246304	0.60000	0.378373	0.137614	0.703346	0.0443546	0.948000	0.616233
0.271548	0.70000	0.432038	0.137828	0.687137	0.0494782	0.925433	0.616894
0.294221	0.80000	0.483866	0.137855	0.671506	0.0541532	0.904293	0.616977
0.314711	0.90000	0.534044	0.137743	0.656521	0.0584352	0.884471	0.616632
0.333333	1.00000	0.582724	0.137528	0.642207	0.0623716	0.865863	0.615969
0.342473	1.05263	0.607789	0.137383	0.634943	0.0643185	0.856522	0.615519
0.352143	1.11111	0.635215	0.137200	0.627086	0.0663890	0.846487	0.614954
0.362396	1.17647	0.665365	0.136973	0.618566	0.0685954	0.835677	0.614254
0.373286	1.25000	0.698684	0.136694	0.609302	0.0709515	0.824000	0.613394
0.384880	1.33333	0.735717	0.136355	0.599199	0.0734735	0.811345	0.612345
0.397253	1.42857	0.777153	0.135943	0.588145	0.0761798	0.797584	0.611072
0.410492	1.53846	0.823862	0.135443	0.576007	0.0790917	0.782562	0.609532
0.424701	1.66667	0.876970	0.134839	0.562626	0.0822344	0.766093	0.607668
0.440001	1.81818	0.937962	0.134108	0.547809	0.0856374	0.747948	0.605413
0.454545	1.97698	1.00000	0.133333	0.533331	0.0888886	0.730295	0.603021
0.456540	2.00000	1.00884	0.133221	0.536015	0.0901254	0.734279	0.602676
0.474496	2.22222	1.09237	0.132139	0.560233	0.101997	0.770589	0.599341
0.494095	2.50000	1.19251	0.130812	0.586789	0.116626	0.811199	0.595251
0.515624	2.85714	1.31517	0.129170	0.616069	0.135040	0.857074	0.590193
0.539464	3.33333	1.46959	0.127114	0.648565	0.158854	0.909552	0.583859
0.566145	4.00000	1.67120	0.124494	0.684923	0.190774	0.970594	0.575792
0.596454	5.00000	1.94831	0.121076	0.726026	0.235754	1.04326	0.565265
0.631682	6.66667	2.35994	0.116446	0.773166	0.304104	1.13287	0.550997
0.674330	10.0000	3.05847	0.109765	0.828464	0.422306	1.25029	0.530357
0.731036	20.0000	4.64473	0.0986983	0.896310	0.693852	1.42650	0.495929

Table 4. Values of effective anisotropy parameters, $\tilde{\zeta}_{33}$, polar axis ratios of non rotating configurations, $(\epsilon_{31})_i$, and polar axis ratios, $(\epsilon_{31})_b$, and normalized rotation parameters, $(\mathcal{E}_{rot})_b$, $(h_N)_b$, $(\upsilon_N)_b$, $(\lambda_N)_b$, $(\chi_N)_b$, of configurations at the bifurcation point, related to sequences of virial equilibrium configurations with constant effective anisotropy parameters. Values at the isotropic ($\tilde{\zeta}_{11} = \tilde{\zeta}_{22} = \tilde{\zeta}_{33}$) are listed on the boldface line.

parameter	NFW	MOA
Ξ	9.20678	3.80693
ν_{mas}	17.05231	8.52616
ν_{inr}	0.0554130	0.0892287
ν_{sel}	0.610045	0.561202
ν_{anm}	0.139180	0.146741
ν_{rot}	0.333333	0.333333
ν_{ram}	17.20783	15.48009

Table 5. Values of the truncated, scaling radius, Ξ, and some profile parameters, expressed in Sect. 2 and particularized to both NFW and MOA density profiles, after comparison with the results of high-resolution simulations (Fukushige & Makino 2001). See text for more details. The last three parameters, related to the rotational velocity field, have been calculated in the special case of constant rotational velocity on the equatorial plane (axisymmetric configurations) related to either rigid ($\eta_{anm} = 2\eta_{rot} = 1$) or differential (to ensure constant rotational velocity everywhere: $\eta_{anm} = 3\pi/8$, $\eta_{rot} = 3/4$) rotation of the generic, isopycnic surface. In the special case of rigidly rotating, triaxial configurations, $\nu_{anm} = \nu_{rot} = \nu_{inr}$, $\nu_{ram} = 1/\nu_{inr}$.

shape factor	limiting configuration						
	p-oblong	f-oblong	flat	f-oblate	prolate	oblate	round
ϵ_{21}	0	0	ϵ_f	1	ϵ_p	1	1
ϵ_{31}	0	0	0	0	ϵ_p	ϵ_o	1
A_1	0	0	0	0	γ	α	2/3
A_2	1	0	0	0	α	α	2/3
A_3	1	2	2	2	α	γ	2/3
$(B_{sel})_{11}$	$+\infty$	$+\infty$	b_1	$\pi/2$	$\epsilon_p^{-2}\gamma$	$\epsilon_o^{-1}\alpha$	2/3
$(B_{sel})_{22}$	1	2	b_2	$\pi/2$	α	$\epsilon_o^{-1}\alpha$	2/3
$(B_{sel})_{33}$	1	0	0	0	α	$\epsilon_o\gamma$	2/3

Table B1. Values of shape factors, A_p and $(B_{sel})_{pp}$, related to limiting configurations defined by the values of the axis ratios, ϵ_{21} and ϵ_{31}.